

Flexible goal-oriented adaptivity for higher-order space-time discretizations of transport problems with coupled flow

Markus Bause^a, Marius Paul Bruchhäuser^{*,a}, Uwe Köcher^a

^a*Helmut Schmidt University, Faculty of Mechanical Engineering, Holstenhofweg 85, 22043 Hamburg*
 bause@hsu-hh.de, bruchhaeuser@hsu-hh.de (* corresponding author),
 koecher@hsu-hh.de.

Abstract

In this work, a flexible higher-order space-time adaptive finite element approximation of convection-dominated transport with coupled fluid flow is developed and studied. Convection-dominated transport is a challenging subproblem in poromechanics in which coupled transport with flow, chemical reaction and mechanical response in porous media is considered. Key ingredients are the arbitrary degree discontinuous Galerkin time discretization of the primal and dual problems for the Dual Weighted Residual (DWR) approach, an a posteriori error estimation for the transport problem coupled with flow and its implementation in an advanced software architecture. The error estimate allows the separation of the temporal and spatial discretization error contributions which facilitates the simultaneous adjustment of the time and space mesh. The performance of the approach and its software implementation is studied by numerical convergence examples as well as an example of physical interest for convection-dominated cases.

Keywords: Space-time adaptivity, goal-oriented a posteriori error control, Dual Weighted Residual method, coupled systems, poromechanics

2019 MSC: 11–30, 01–25

1. Introduction

Coupling convection-dominated transport with flow, chemical reaction and mechanical response in porous media with or without fracture development has attracted researcher's interest for many years and receives increasing interest currently; cf. [1, 2, 3, 4, 5, 6, 7, 8]. The strong multi-physics character of the models of coupled transport, flow, deformation and fracture propagation yields, for instance, different time scales such that iterative coupling methods and multi-rate time discretizations are broadly used and studied; cf. [5, 9, 10, 11]. The governing system of a single-phase convection-diffusion transport reads as

$$\partial_t(\phi \rho(p) u) + \nabla \cdot (\rho(p) u \mathbf{v} - \phi \rho(p) \mathbf{D}(\mathbf{v}) \nabla u) = g, \quad (1.1)$$

with the unknown concentration variable u which is transported by a convection-diffusion process with the convection tensor \mathbf{v} and the diffusion tensor \mathbf{D} . The other variables in Eq. (1.1) are the porosity $\phi \in (0, 1]$, the mass density $\rho > 0$, the fluid pressure p and the source term g of the transport equation. Here, we consider a linearized tensor of the type $\mathbf{D} = \varepsilon \mathbf{I}$ with a scalar diffusion parameter ε . Dispersion effects are neglectable for convection-dominated transport. The Navier-Stokes equations of a flow model read as

$$\partial_t \mathbf{v} - 2\tilde{\nu}(\nabla \cdot \boldsymbol{\epsilon}(\mathbf{v})) + (\mathbf{v} \cdot \nabla) \mathbf{v} + \nabla p = \mathbf{f}, \quad \nabla \cdot \mathbf{v} = 0,$$

for the fluid convection \mathbf{v} and pressure p variables and the viscosity $\tilde{\nu}$. This flow model is simplified here to the quasi-static Stokes equations

$$-\nu \Delta \mathbf{v} + \nabla p = \mathbf{f} \quad (1.2)$$

of an incompressible fluid $\nabla \cdot \mathbf{v} = 0$ due to the assumption of a slow moving viscous fluid. The latter assumption comes from our focus on a highly time-dynamic transport in a porous media with very small diffusion relative to the convection. Thus, our linear transport problem yields a singularly-disturbed linear transport problem with the typical issue of numerical oscillations. In poromechanics the quasi-static or dynamic mechanical response model is coupled very often in an iterative way to transport and flow models; cf. e.g. [11] and references therein. For completeness, we give here the extension of the governing transport model from Eqs. (1.1)-(1.2) with the quasi-static Biot's equations as

$$-\nabla \cdot \boldsymbol{\sigma}(\mathbf{u}_m) + \alpha \nabla p = \mathbf{f}_m$$

for the mechanical deformation \mathbf{u}_m due to fluid and capillary pressure and time-dependent mechanical forcing changes. The mechanical stress is denoted by $\boldsymbol{\sigma}$ and α is the Biot-Willis model-coupling parameter. This

mechanical equilibrium equation is supported by the additional Darcy transport system

$$\partial_t(c_0 p + \alpha(\nabla \cdot \mathbf{u}_m)) + \nabla \cdot \mathbf{v}_D = q, \quad \mathbf{v}_D = \boldsymbol{\kappa}(-\nabla p + \rho_f \mathbf{g}),$$

with a storage coefficient c_0 , the Darcy velocity \mathbf{v}_D , a source term q , a viscosity-permeability tensor $\boldsymbol{\kappa}$, the fluid density ρ_f and the gravity \mathbf{g} . The latter Darcy transport equation is of the same structure as Eq. (1.1) with $\epsilon_v := \nabla \cdot \mathbf{u}_m$, \mathbf{u}_m and \mathbf{v}_D depending on the pressure p , and the first equation of the Stokes system (1.2) is similar to the quasi-static equilibrium equation of the Biot's system.

The numerical approximation of convection-dominated transport problems (1.1) and incompressible flow (1.2) remains a challenging task, cf. [12] and references therein. In (1.1), convection-dominated transport is comprised by assuming that $0 < \varepsilon \ll |\mathbf{v}|$. The solution of these transport problems are typically characterized by the occurrence of sharp moving fronts and layers. The key challenge for the numerical approximation exists in the accurate and efficient solution while avoiding non-physical oscillations or smearing effects. The application of stabilization techniques is a typical approach to overcome non-physical effects. As shown in a comparative study for time-dependent convection-diffusion-reaction equations in [13], stabilization techniques on globally refined meshes fail to avoid these oscillations even after tuning stabilization parameters. For a general review of stabilization techniques we refer to [14, 12].

Furthermore, the non-availability of parameter-robust a posteriori error estimates for quantities of physical interest and in general situations is complained in [12]. Moreover, the authors point out that adaptive mesh refinement strategies that are based on such a posteriori error estimates are desirable and indispensable for further improvement.

One possible technique for those adaptive strategies is goal-oriented a posteriori error control. For a general review of a posteriori error estimation we refer to [15, 16]. In particular, the Dual Weighted Residual (DWR) method, introduced by Becker and Rannacher [17, 18, 19], allows for goal-oriented error control and adaptive mesh refinement by weighting the influence of local residuals on the error within a goal quantity of physical relevance. The DWR approach relies on a space-time variational formulation of the discrete problem and uses duality techniques to find a rigorous a posteriori error estimate through the approximation of an addition dual problem. Since the pioneering work in duality based error estimation, numerous studies have been done for the application of the DWR method to several classes of problems of physics including coupled phenomena and problems of optimal control. Generalized versions of the DWR method in that not only the discretization error but also the iteration or a modelling error is addressed, have been developed and studied; cf. [20, 21]. Further generalizations consider multi-objective goal functionals and the treatment of higher-order corrections of the error estimator that are often neglected; cf. [22, 23]. In [22], error localization of the DWR method is performed in a variational form using a partition-of-unity approach, instead of evaluating strong operators and face integrals, as it is done in the classical way of error localization [24]. Thereby, node-wise error contributions are obtained and computational costs are reduced.

DWR based error control has been well understood for single-physics problems. Rigorous studies of DWR techniques for nonstationary multi-physics systems and their numerical validations are still rare in the literature. One reason for this might be that the separation of contributions to the discretization error and the control of the temporal and spatial mesh becomes more involved since, in addition, the impact of each of the subproblems and its approximation on the goal quantity has to be understood and balanced within the localized error representation and mesh refinement process. In particular, goal-oriented error control was strongly analyzed for the computation of nonstationary incompressible flow modeled by the Navier–Stokes equations; cf. [25, 26] and references therein. Moreover, the economical simulation of fluid-structure interaction as a prominent system of multi-physics has attracted the usage of a posteriori error control mechanisms based on duality techniques; cf. [27, 28, 29]. A goal-oriented spatial-only adaptivity for a nonstationary transport problem coupled with a stationary Darcy flow, which is related to this work, is studied in [1].

Finally, we note that the efficiency of goal-oriented space-time adaptive methods demands on their efficient software implementation. This requires the appropriate selection and implementation, respectively, of data structures and efficient algorithms acting on them. Recently, a programming model for the DWR approach applied to the nonstationary diffusion equation with fixed lowest-order time discretizations for the primal and dual problem was published by the authors in [30].

In this work we combine the DWR approach with streamline upwind Petrov-Galerkin (SUPG) stabilized approximations of convection-dominated transport problems as introduced by Eq. (1.1). The transport problem is coupled via a convection tensor obtained by an auxiliary flow problem as given by Eq. (1.2) that has to be solved additionally. Precisely, this work is characterised by the following features.

- An arbitrary order discontinuous Galerkin (dG) time discretization is rigorously applied to the primal and dual problem.
- The automatic adaptation of the space and time mesh is simplified by separating the errors of temporal and spatial discretization similar to the approach given in [25, 31].

- The dual residual is computed explicitly for both error representations, the error in space and time, similarly to, e.g., [25, 31].
- A new software based on tensor-product space-time slabs was developed. Further, the Stokes solver is an encapsulated module providing the convection tensor for the convection-diffusion transport problem working on a different triangulation. This is an extension of the software used in [30].

This work is organized as follows. In Sec. 2 we present the space-time discretization of our model problem, including its stabilization for convection-dominated transport. In Sec. 3 the DWR method is applied and localized a posteriori error representations, separating the effects of temporal and spatial discretization, are derived. In Sec. 4 the underlying adaptive algorithm is presented, some practical aspects for the realization of the adaptivity process are illustrated and details of the software implementation are given. In Sec. 5 the numerical performance properties are studied with convergence tests and a sophisticated experiment of physical relevance is studied. Finally, in Sec. 6 we summarize and give some outlook for future work.

2. Model problem and stabilized space-time discretization

In this section we briefly introduce the space-time finite element discretization of (1.1), (1.2) including the SUPG stabilization to capture convection-dominated transport.

2.1. Model problem

The time dependent convection-diffusion transport problem is given by

$$\rho \partial_t u - \nabla \cdot (\varepsilon \nabla u) + \mathbf{v} \cdot \nabla u + \alpha u = g \quad \text{in } Q = \Omega \times I, \quad (2.1a)$$

$$u = 0 \quad \text{on } \Sigma_D = \partial\Omega \times I, \quad (2.1b)$$

$$u = u_0 \quad \text{on } \Sigma_0 = \Omega \times \{0\}, \quad (2.1c)$$

with the coupled Stokes flow

$$-\nu \Delta \mathbf{v} + \nabla p = \mathbf{f} \quad \text{in } \Omega, \quad (2.2a)$$

$$\nabla \cdot \mathbf{v} = 0 \quad \text{in } \Omega, \quad (2.2b)$$

equipped with appropriate boundary conditions. The system (2.1), (2.2) is studied due to its prototype character for a wide range of applications in practice, as introduced in Sec. 1. In particular, its use for poroelasticity models and poromechanics in a more general sense is straightforward. The goal-oriented adaptivity approach that is developed in this work is general enough such that it can be adapted to multi-physics systems.

In (2.1), (2.2), we denote by $\Omega \subset \mathbb{R}^d$, with $d = 2, 3$, a polygonal or polyhedral bounded domain with Lipschitz boundary $\partial\Omega$ and $I = (0, T]$, $0 < T < \infty$, is a finite time interval. We assume that $\varepsilon > 0$ is a constant diffusion coefficient, $\alpha \in L^\infty(\Omega)$ is the reaction coefficient, $\rho > 0$ is the constant density coefficient and $\nu > 0$ is the constant viscosity coefficient. Homogeneous Dirichlet boundary conditions in the transport and flow problem are prescribed for brevity only. In our numerical examples in Sec. 5 we also consider more general boundary conditions. For the sake of physical realism, the transport problem is supposed to be convection-dominated by the at least local condition of $0 < \varepsilon \ll |\mathbf{v}|$. Well-posedness of (2.1), (2.2) and the existence of a sufficiently regular solution, such that all of the arguments and terms used below are well-defined, are tacitly assumed without mentioning explicitly all technical assumptions about the data and coefficients.

2.2. Weak formulation

Let $X := \{v \in L^2(0, T; H_0^1(\Omega)) \mid \partial_t v \in L^2(0, T; H^{-1}(\Omega))\}$ and $Y_1 := H_0^1(\Omega)^d$. The weak formulation of (2.1) reads as follows: Find $u \in X$, $\mathbf{v} \in Y_1$ such that

$$A(u, \mathbf{v})(\varphi) = G(\varphi) \quad \forall \varphi \in X, \quad (2.3)$$

where the bilinear form $A : \{X, Y_1\} \times X \rightarrow \mathbb{R}$ and the linear form $G : L^2(0, T; H^{-1}(\Omega)) \rightarrow \mathbb{R}$ are defined by

$$A(u, \mathbf{v})(\varphi) := \int_I \{(\rho \partial_t u, \varphi) + a(u, \mathbf{v})(\varphi)\} dt + (u(0), \varphi(0)),$$

$$G(\varphi) := \int_I (g, \varphi) dt + (u_0, \varphi(0)),$$

with the bilinear form $a : \{H_0^1(\Omega), H_0^1(\Omega)^d\} \times H_0^1(\Omega) \rightarrow \mathbb{R}$ given by

$$a(u, \mathbf{v})(\varphi) := (\varepsilon \nabla u, \nabla \varphi) + (\mathbf{v} \cdot \nabla u, \varphi) + (\alpha u, \varphi). \quad (2.4)$$

Here, (\cdot, \cdot) denotes the inner product of $L^2(\Omega)$ or duality pairing of $H^{-1}(\Omega)$ with $H_0^1(\Omega)$, respectively. By $\|\cdot\|$ we denote the associated L^2 -norm.

For the variational formulation of problem (2.2) we define $Y_2 := L_0^2(\Omega) := \{p \in L^2(\Omega) \mid \int_{\Omega} p \, d\mathbf{x} = 0\}$. Then we get: For $\mathbf{f} \in H^{-1}(\Omega)^d$ find $\{\mathbf{v}, p\} \in Y := Y_1 \times Y_2 = H_0^1(\Omega)^d \times L_0^2(\Omega)$, such that

$$B(\mathbf{v}, p)(\boldsymbol{\psi}, \chi) = F(\boldsymbol{\psi}) \quad \forall \{\boldsymbol{\psi}, \chi\} \in Y, \quad (2.5)$$

where the bilinear form $B : Y \times Y \rightarrow \mathbb{R}$ and the linear form $F : H^{-1}(\Omega)^d \rightarrow \mathbb{R}$ are defined by

$$B(\mathbf{v}, p)(\boldsymbol{\psi}, \chi) := \nu(\nabla \mathbf{v}, \nabla \boldsymbol{\psi}) - (p, \nabla \cdot \boldsymbol{\psi}) + (\nabla \cdot \mathbf{v}, \chi), \quad (2.6a)$$

$$F(\boldsymbol{\psi}) := (\mathbf{f}, \boldsymbol{\psi}). \quad (2.6b)$$

Remark 2.1. The coupling of the transport problem with the stationary Stokes problem is via the convection variable \mathbf{v} of the system (2.1), (2.2). We consider for the error estimation in Sec. 3 a coupled system but remark that the coupling is uni-directional from the Stokes to the transport problem.

2.3. Discretization in time

For the discretization in time of the transport problem (2.3) we use a discontinuous Galerkin method dG(r) with an arbitrary polynomial degree $r \geq 0$. Let $0 =: t_0 < t_1 < \dots < t_N := T$ be a partition of the closure of the time domain $\bar{I} = [0, T]$ into left-open subintervals $I_n := (t_{n-1}, t_n]$, $n = 1, \dots, N$, with time step sizes $\tau_n = t_n - t_{n-1}$ and the global time discretization parameter $\tau = \max_n \tau_n$. Therefore, we introduce the time-discrete function space $X_{\tau}^{\text{dG}(r)}$ for the transport problem.

$$X_{\tau}^{\text{dG}(r)} := \left\{ u_{\tau} \in L^2(I; H_0^1(\Omega)) \mid u_{\tau}|_{I_n} \in \mathcal{P}_r(I_n; H_0^1(\Omega)), \right. \\ \left. u_{\tau}(0) \in L^2(\Omega), n = 1, \dots, N \right\}, \quad (2.7)$$

where $\mathcal{P}_r(\bar{I}_n; H_0^1(\Omega))$ denotes the space of all polynomials in time up to degree $r \geq 0$ on I_n with values in $H_0^1(\Omega)$.

For some discontinuous in time function $u_{\tau} \in X_{\tau}^{\text{dG}(r)}$ we define the limits $u_{\tau, n}^{\pm}$ from above and below of u_{τ} at t_n as well as their jump at t_n by

$$u_{\tau, n}^{\pm} := \lim_{t \rightarrow t_n \pm 0} u_{\tau}(t), \quad [u_{\tau}]_n := u_{\tau, n}^+ - u_{\tau, n}^-.$$

The semidiscretization in time of the the transport problem (2.3) then reads as follows: Find $u_{\tau} \in X_{\tau}^{\text{dG}(r)}$, $\mathbf{v} \in Y_1$ such that

$$A_{\tau}(u_{\tau}, \mathbf{v})(\varphi_{\tau}) = G_{\tau}(\varphi_{\tau}) \quad \forall \varphi_{\tau} \in X_{\tau}^{\text{dG}(r)}, \quad (2.8)$$

where the semi-discrete bilinear form and linear form are given by

$$A_{\tau}(u_{\tau}, \mathbf{v})(\varphi_{\tau}) := \sum_{n=1}^N \int_{I_n} \{(\rho \partial_t u_{\tau}, \varphi_{\tau}) + a(u_{\tau}, \mathbf{v})(\varphi_{\tau})\} dt \quad (2.9a)$$

$$+ \sum_{n=2}^N (\rho [u_{\tau}]_{n-1}, \varphi_{\tau, n-1}^+) + (\rho u_{\tau, 0}^+, \varphi_{\tau, 0}^+), \\ G_{\tau}(\varphi_{\tau}) := \int_I (g, \varphi_{\tau}) \, dt + (u_0, \varphi_{\tau, 0}^+). \quad (2.9b)$$

2.4. Discretization in space

Next, we describe the Galerkin finite element approximation in space of the semi-discrete transport problem (2.8) and the flow problem (2.5), respectively. We use Lagrange type finite element spaces of continuous functions that are piecewise polynomials. For the discretization in space, we consider a decomposition \mathcal{T}_h of the domain Ω into disjoint elements K , such that $\bar{\Omega} = \cup_{K \in \mathcal{T}_h} \bar{K}$. Here, we choose the elements $K \in \mathcal{T}_h$ to be quadrilaterals for $d = 2$ and hexahedrals for $d = 3$. We denote by h_K the diameter of the element K . The global space discretization parameter h is given by $h := \max_{K \in \mathcal{T}_h} h_K$. Our mesh adaptation process yields locally refined cells, which is enabled by using hanging nodes. We point out that the global conformity of the finite element approach is preserved since the unknowns at such hanging nodes are eliminated by interpolation between the neighboring 'regular' nodes; cf. [24, Chapter 4.2] and [32] for more details. On \mathcal{T}_h we define the discrete finite element space by $V_h^{p, n} := \{v \in C(\bar{\Omega}) \mid v|_K \in Q_h^p(K), \forall K \in \mathcal{T}_h, \}$, with $n = 1, \dots, N$, where $Q_h^p(K)$ is the space defined on the reference element with maximum degree p in each variable. By replacing $H_0^1(\Omega)$ in the definition

of the semi-discrete function space $X_\tau^{\text{dG}(r)}$ in (2.7) by $V_h^{p,n}$, we obtain the fully discrete function space for the transport problem

$$X_{\tau h}^{\text{dG}(r),p} := \left\{ u_{\tau h} \in X_\tau^{\text{dG}(r)} \mid u_{\tau h}|_{I_n} \in \mathcal{P}_r(I_n; H_h^{p_u,n}), \right. \\ \left. u_{\tau h}(0) \in H_h^{p_u,0}, n = 1, \dots, N \right\} \subseteq L^2(I; H_0^1(\Omega)). \quad (2.10)$$

The discrete in space function space for the flow problem is given by

$$Y_h^p := (H_h^{p_v})^d \times L_h^{p_p} \subseteq Y, \quad (2.11)$$

$$H_h^{p_u,n} := V_h^{p_u,n} \cap H_0^1(\Omega), \quad H_h^{p_v} := V_h^{p_v} \cap H_0^1(\Omega), \quad L_h^{p_p} := V_h^{p_p} \cap L_0^2(\Omega).$$

We note that the spatial finite element space $V_h^{p,n}$ is allowed to be different on all subintervals I_n which is natural in the context of a discontinuous Galerkin approximation of the time variable and allows dynamic mesh changes in time. Due to the conformity of $H_h^{p_u,n}$ we get $X_{\tau h}^{\text{dG}(r),p} \subseteq X_\tau^{\text{dG}(r)}$.

The fully discrete discontinuous in time scheme for the transport problem then reads as follows: *Find* $u_{\tau h} \in X_{\tau h}^{\text{dG}(r),p}$, $\mathbf{v}_h \in (H_h^{p_v})^d$ *such that*

$$A_\tau(u_{\tau h}, \mathbf{v}_h)(\varphi_{\tau h}) = G_\tau(\varphi_{\tau h}) \quad \forall \varphi_{\tau h} \in X_{\tau h}^{\text{dG}(r),p}, \quad (2.12)$$

with $A_\tau(\cdot, \cdot)(\cdot)$ and $G_\tau(\cdot)$ being defined in (2.9). We note that the bilinear form $a(\cdot, \cdot)(\cdot)$ occurring in $A_\tau(\cdot, \cdot)(\cdot)$ reads here as

$$a(u_{\tau h}, \mathbf{v}_h)(\varphi_{\tau h}) = (\varepsilon \nabla u_{\tau h}, \nabla \varphi_{\tau h}) + (\mathbf{v}_h \cdot \nabla u_{\tau h}, \varphi_{\tau h}) + (\alpha u_{\tau h}, \varphi_{\tau h})$$

for the fully discrete solutions.

The fully discrete scheme for the flow problem reads as follows: *Find* $\{\mathbf{v}_h, p_h\} \in Y_h^p$ *such that*

$$B(\mathbf{v}_h, p_h)(\psi_h, \chi_h) = F(\psi_h) \quad \forall \{\psi_h, \chi_h\} \in Y_h^p, \quad (2.13)$$

with $B(\cdot, \cdot)(\cdot, \cdot)$ and $F(\cdot)$ being defined in (2.6).

2.5. SUPG stabilization

In this work we consider, for the sake of physical realism, convection-dominated transport with small diffusion parameter ε in Eq. (2.1) which, on the hand, poses an additional challenge to the a posteriori error control but, on the other hand, illustrates nicely the potential, reliability and efficiency of the DWR-based approach. For convection-dominated transport, the finite element approximation needs to be stabilized in order to further reduce spurious and non-physical oscillations of the discrete solution arising close to sharp fronts or layers. Here, we apply the streamline upwind Petrov-Galerkin (SUPG) method; cf. [33, 34]. We explicitly note that SUPG stabilization and automatic mesh adaptation interact strongly; cf. Rem. 2.2. Balancing their effects needs particular consideration and has not been strongly studied so far in the literature; cf. for instance [35].

The stabilized variant of the fully discrete scheme (2.12) then reads as follows: *Find* $u_{\tau h} \in X_{\tau h}^{\text{dG}(r),p}$, $\mathbf{v}_h \in (H_h^{p_v})^d$ *such that*

$$A_S(u_{\tau h}, \mathbf{v}_h)(\varphi_{\tau h}) = G_\tau(\varphi_{\tau h}) \quad \forall \varphi_{\tau h} \in X_{\tau h}^{\text{dG}(r),p}, \quad (2.14)$$

with $A_S(u_{\tau h}, \mathbf{v}_h)(\varphi_{\tau h}) := A_\tau(u_{\tau h}, \mathbf{v}_h)(\varphi_{\tau h}) + S(u_{\tau h}, \mathbf{v}_h)(\varphi_{\tau h})$ and stabilization term

$$S(u_{\tau h}, \mathbf{v}_h)(\varphi_{\tau h}) := \sum_{n=1}^N \int_{I_n} \sum_{K \in \mathcal{T}_h} \delta_K(r(u_{\tau h}, \mathbf{v}_h), \mathbf{v}_h \cdot \nabla \varphi_{\tau h})_K \, dt \\ + \sum_{n=2}^N \sum_{K \in \mathcal{T}_h} \delta_K(\rho[u_{\tau h}]_{n-1}, \mathbf{v}_h \cdot \nabla \varphi_{\tau h, n-1}^+)_K \\ + \sum_{K \in \mathcal{T}_h} \delta_K(\rho u_{\tau h, 0}^+ - u_0, \mathbf{v}_h \cdot \nabla \varphi_{\tau h, 0}^+)_K \quad (2.15)$$

and residual

$$r(u_{\tau h}, \mathbf{v}_h) := \rho \partial_t u_{\tau h} - \nabla \cdot (\varepsilon \nabla u_{\tau h}) + \mathbf{v}_h \cdot \nabla u_{\tau h} + \alpha u_{\tau h} - g.$$

Remark 2.2. The proper choice of the stabilization parameter δ_K is an important issue in the application of the SUPG approach; cf., e.g., [36, 13, 12] and the discussion therein. For time-dependent convection-diffusion-reaction problems an optimal error estimate for $\delta_K = O(h)$ is derived in [36].

Remark 2.3. For the error $e = u_\tau - u_{\tau h}$ we get by subtracting Eq. (2.14) from Eq. (2.8) the identity

$$\begin{aligned} & \sum_{n=1}^N \int_{I_n} \{(\rho \partial_t e, \varphi_{\tau h}) + a(e, \mathbf{v}_h)(\varphi_{\tau h})\} dt \\ & + \sum_{n=2}^N (\rho [e]_{n-1}, \varphi_{\tau h, n-1}^+) + (e_0^+, \varphi_{\tau h, 0}^+) \\ & = S(u_{\tau h}, \mathbf{v}_h)(\varphi_{\tau h}) - \sum_{n=1}^N \int_{I_n} ((\mathbf{v} - \mathbf{v}_h) \cdot \nabla u_\tau, \varphi_{\tau h}) dt, \end{aligned} \quad (2.16)$$

with a non-vanishing right-hand side term depending on the stabilization and the error in the approximation of the flow field. Eq. (2.16) with the perturbation term on the right-hand side replaces the standard Galerkin orthogonality of the space-time finite element approximation.

3. A posteriori error estimation

In this section we derive our DWR error representation for the stabilized transport problem (2.14) coupled with the flow problem via the convection tensor \mathbf{v}_h given by Eq. (2.13). Here, only goal quantities depending on the unknown u are studied. For applications of practical interest, physical quantities in terms of the transport quantity u are typically of higher relevance than quantities in the unknowns \mathbf{v} and p of the flow problem. In the sequel, we denote by $J : X \rightarrow \mathbb{R}$ a user-chosen, physically relevant target functional represented in the form

$$J(u) = \int_0^T J_1(u(t)) dt + J_2(u(T)), \quad (3.1)$$

where $J_1 : H_0^1(\Omega) \rightarrow \mathbb{R}$ or $J_2 : H_0^1(\Omega) \rightarrow \mathbb{R}$ may be zero. Since we aim at controlling the respective errors due to the discretization in time as well as in space, we split the a posteriori error representation with respect to J into the contributions

$$J(u) - J(u_{\tau h}) = J(u) - J(u_\tau) + J(u_\tau) - J(u_{\tau h}). \quad (3.2)$$

For the respective error representations we define the Lagrangian functionals $\mathcal{L} : X \times X \rightarrow \mathbb{R}$, $\mathcal{L}_\tau : X_\tau^{\text{dG}(r)} \times X_\tau^{\text{dG}(r)} \rightarrow \mathbb{R}$, and $\mathcal{L}_{\tau h} : X_{\tau h}^{\text{dG}(r), p} \times X_{\tau h}^{\text{dG}(r), p} \rightarrow \mathbb{R}$ by

$$\mathcal{L}(u, z) := J(u) + G(z) - A(u, \mathbf{v})(z), \quad (3.3a)$$

$$\mathcal{L}_\tau(u_\tau, z_\tau) := J(u_\tau) + G_\tau(z_\tau) - A_\tau(u_\tau, \mathbf{v})(z_\tau), \quad (3.3b)$$

$$\mathcal{L}_{\tau h}(u_{\tau h}, z_{\tau h}) := J(u_{\tau h}) + G_\tau(z_{\tau h}) - A_S(u_{\tau h}, \mathbf{v}_h)(z_{\tau h}). \quad (3.3c)$$

Here, the Lagrange multipliers z , z_τ , and $z_{\tau h}$ are called dual variables in contrast to the primal variables u , u_τ , and $u_{\tau h}$; cf. [25, 19].

Remark 3.1. For the sake of simplicity, we exclude the convection field \mathbf{v} and \mathbf{v}_h from the primal variables within the Lagrangian functionals in (3.3) due to the choice of the goal quantity given by Eq. (3.1). This can be generalized in a standard fashion by introducing a vector of primal unknowns and a respective Lagrangian multiplier as dual variable. Nevertheless, the coupling is still present within the transport problem and results in additional coupling terms in the error representation formula, cf. Eq. (3.16b) and Rem. 3.3.

Considering the directional derivatives of the Lagrangian functionals, also known as Gâteaux derivatives, with respect to their first argument, i.e.

$$\mathcal{L}'_u(u, z)(\varphi) := \lim_{t \neq 0, t \rightarrow 0} t^{-1} \{ \mathcal{L}(u + t\varphi, z) - \mathcal{L}(u, z) \}, \quad \varphi \in X, \quad (3.4)$$

leads to the so-called dual problems, cf., e.g., [25]. The continuous, semi-discrete, and fully discrete dual solutions $z \in X$, $z_\tau \in X_\tau^{\text{dG}(r)}$, and $z_{\tau h} \in X_{\tau h}^{\text{dG}(r), p}$ are determined by the optimality conditions

$$\mathcal{L}'_u(u, z)(\varphi) = 0 \quad \forall \varphi \in X, \quad (3.5a)$$

$$\mathcal{L}'_{\tau, u}(u_\tau, z_\tau)(\varphi) = 0 \quad \forall \varphi_\tau \in X_\tau^{\text{dG}(r)}, \quad (3.5b)$$

$$\mathcal{L}'_{\tau h, u}(u_{\tau h}, z_{\tau h})(\varphi) = 0 \quad \forall \varphi_{\tau h} \in X_{\tau h}^{\text{dG}(r), p}. \quad (3.5c)$$

More precisely, the continuous dual solution $z \in X$ is the solution of

$$A'(u, \mathbf{v})(\varphi, z) = J'(u)(\varphi) \quad \forall \varphi \in X, \quad (3.6)$$

where the adjoint bilinear form $A'(\cdot, \cdot)(\cdot, \cdot)$ is given by

$$A'(u, \mathbf{v})(\varphi, z) := \int_I \{(\varphi, -\rho \partial_t z) + a'(u, \mathbf{v})(\varphi, z)\} dt + (\varphi(T), z(T)). \quad (3.7)$$

We note that for the representation (3.7) of $A'(\cdot, \cdot)(\cdot, \cdot)$ integration by parts in time is applied, which is allowed for weak solutions $z \in X$; cf., e.g., [27, Lemma 8.9]. The derivative $a'(u, \mathbf{v})(\varphi, z)$ of the bilinear form $a(u, \mathbf{v})(z)$ in A' admits the explicit form

$$a'(u, \mathbf{v})(\varphi, z) = (\varepsilon \nabla \varphi, \nabla z) + (\mathbf{v} \cdot \nabla \varphi, z) + (\alpha \varphi, z).$$

The right-hand side of Eq. (3.6) is given by

$$J'(u)(\varphi) := \int_I J'_1(u)(\varphi) dt + J'_2(u(T))(\varphi(T)). \quad (3.8)$$

Further, the semi-discrete dual solution $z_\tau \in X_\tau^{\text{dG}(r)}$ and the fully discrete dual solution $z_{\tau h} \in X_{\tau h}^{\text{dG}(r), p}$ satisfy the equations

$$A'_\tau(u_\tau, \mathbf{v})(\varphi_\tau, z_\tau) = J'(u_\tau)(\varphi_\tau) \quad \forall \varphi_\tau \in X_\tau^{\text{dG}(r)}, \quad (3.9a)$$

$$A'_S(u_{\tau h}, \mathbf{v}_h)(\varphi_{\tau h}, z_{\tau h}) = J'(u_{\tau h})(\varphi_{\tau h}) \quad \forall \varphi_{\tau h} \in X_{\tau h}^{\text{dG}(r), p}, \quad (3.9b)$$

where $A'_\tau(\cdot, \cdot)(\cdot, \cdot)$ and $A'_S(\cdot, \cdot)(\cdot, \cdot)$ are given by

$$\begin{aligned} A'_\tau(u_\tau, \mathbf{v})(\varphi_\tau, z_\tau) &:= \sum_{n=1}^N \int_{I_n} \{(\varphi_\tau, -\rho \partial_t z_\tau) + a'(u_\tau, \mathbf{v})(\varphi_\tau, z_\tau)\} dt \\ &\quad - \sum_{n=1}^{N-1} (\varphi_{\tau, n}^-, \rho [z_\tau]_n) + (\varphi_{\tau, N}^-, \rho z_{\tau, N}^-), \end{aligned}$$

and

$$\begin{aligned} A'_S(u_{\tau h}, \mathbf{v}_h)(\varphi_{\tau h}, z_{\tau h}) &:= \sum_{n=1}^N \int_{I_n} \{(\varphi_{\tau h}, -\rho \partial_t z_{\tau h}) + a'_h(u_{\tau h}, \mathbf{v}_h)(\varphi_{\tau h}, z_{\tau h})\} dt \\ &\quad + S'(u_{\tau h}, \mathbf{v}_h)(\varphi_{\tau h}, z_{\tau h}) - \sum_{n=1}^{N-1} (\varphi_{\tau h, n}^-, \rho [z_{\tau h}]_n) + (\varphi_{\tau h, N}^-, \rho z_{\tau h, N}^-). \end{aligned}$$

Remark 3.2. We note that the directional derivatives of the Lagrangian functionals with respect to their second argument leads to the primal problems given by Eqs. (2.3), (2.8) and (2.14), respectively.

For the derivation of computable representations of the separated error contributions in Eq. (3.2) we need the following known result, that is explicitly summarized here in order to keep this work self-contained.

Lemma 3.1. *Let \mathcal{Y} be a function space and L and \tilde{L} be three times Gâteaux differentiable functionals on \mathcal{Y} . We seek a stationary point y_1 of L on a subspace $\mathcal{Y}_1 \subseteq \mathcal{Y}$: Find $y_1 \in \mathcal{Y}_1$ such that*

$$L'(y_1)(\delta y_1) = 0 \quad \forall \delta y_1 \in \mathcal{Y}_1. \quad (3.10)$$

This equation is approximated by a Galerkin method using the functional \tilde{L} on a subspace $\mathcal{Y}_2 \subseteq \mathcal{Y}$. Hence, the discrete problem seeks $y_2 \in \mathcal{Y}_2$ such that

$$\tilde{L}'(y_2)(\delta y_2) = 0 \quad \forall \delta y_2 \in \mathcal{Y}_2. \quad (3.11)$$

If the continuous solution y_1 additionally fulfills

$$L'(y_1)(y_2) = 0, \quad (3.12)$$

with the approximated solution y_2 , we have the error representation

$$\begin{aligned} L(y_1) - \tilde{L}(y_2) &= \frac{1}{2} L'(y_2)(y_1 - \tilde{y}_2) \\ &\quad + \frac{1}{2} (L - \tilde{L})'(y_2)(\tilde{y}_2 - y_2) + (L - \tilde{L})(y_2) + \mathcal{R}, \end{aligned} \quad (3.13)$$

for arbitrary $\tilde{y}_2 \in \mathcal{Y}_2$, where the remainder term \mathcal{R} is given in terms of $e := y_1 - y_2$ as

$$\mathcal{R} = \frac{1}{2} \int_0^1 L'''(y_2 + se)(e, e, e) s(s-1) ds. \quad (3.14)$$

Proof. The proof of Lemma 3.1 can be found in [25]. \square

In the following Thm. 3.1 we apply the abstract error representation formula (3.13) to the Lagrangian functionals (3.3a)–(3.3c). This step is a modification of Thm. 5.2 in [25] due to the presence of the additional coupling term, cf. Rem. 2.3. To proceed with our computations, we still introduce the primal and dual residuals that are defined by means of

$$\rho_t(u)(\varphi) := \mathcal{L}'_{\tau,z}(u, z)(\varphi), \quad \rho_t^*(u, z)(\varphi) := \mathcal{L}'_{\tau,u}(u, z)(\varphi). \quad (3.15)$$

By using Lemma 3.1 we now get the following result for the DWR-based error representation.

Theorem 3.1. *Let $\{u, z\} \in X \times X$, $\{u_\tau, z_\tau\} \in X_\tau^{\text{dG}(r)} \times X_\tau^{\text{dG}(r)}$, and $\{u_{\tau h}, z_{\tau h}\} \in X_{\tau h}^{\text{dG}(r),p} \times X_{\tau h}^{\text{dG}(r),p}$ denote the stationary points of $\mathcal{L}, \mathcal{L}_\tau$, and $\mathcal{L}_{\tau h}$ on the different levels of discretization, i.e.,*

$$\begin{aligned} \mathcal{L}'(u, z)(\delta u, \delta z) &= \mathcal{L}'_\tau(u, z)(\delta u, \delta z) = 0 \quad \forall \{\delta u, \delta z\} \in X \times X, \\ \mathcal{L}'_\tau(u_\tau, z_\tau)(\delta u_\tau, \delta z_\tau) &= 0 \quad \forall \{\delta u_\tau, \delta z_\tau\} \in X_\tau^{\text{dG}(r)} \times X_\tau^{\text{dG}(r)}, \\ \mathcal{L}'_{\tau h}(u_{\tau h}, z_{\tau h})(\delta u_{\tau h}, \delta z_{\tau h}) &= 0 \quad \forall \{\delta u_{\tau h}, \delta z_{\tau h}\} \in X_{\tau h}^{\text{dG}(r),p} \times X_{\tau h}^{\text{dG}(r),p}. \end{aligned}$$

Additionally, for the error $e = u_\tau - u_{\tau h}$ we have the Eq. (2.16) of Galerkin orthogonality type. Then, for the discretization errors in space and time we get the representation formulas

$$J(u) - J(u_\tau) = \frac{1}{2}\rho_t(u_\tau)(z - \tilde{z}_\tau) + \frac{1}{2}\rho_t^*(u_\tau, z_\tau)(u - \tilde{u}_\tau) + \mathcal{R}_\tau, \quad (3.16a)$$

$$\begin{aligned} J(u_\tau) - J(u_{\tau h}) &= \frac{1}{2}\rho_t(u_{\tau h})(z_\tau - \tilde{z}_{\tau h}) + \frac{1}{2}\rho_t^*(u_{\tau h}, z_{\tau h})(u_\tau - \tilde{u}_{\tau h}) \\ &\quad + \frac{1}{2}\mathcal{D}'_{\tau h}(u_{\tau h}, z_{\tau h})(\tilde{u}_{\tau h} - u_{\tau h}, \tilde{z}_{\tau h} - z_{\tau h}) \\ &\quad + \mathcal{D}_{\tau h}(u_{\tau h}, z_{\tau h}) + \mathcal{R}_h, \end{aligned} \quad (3.16b)$$

where $\mathcal{D}_{\tau h}(\cdot, \cdot)$ is given by

$$\mathcal{D}_{\tau h}(\varphi, \psi) = S(\varphi, \mathbf{v}_h)(\psi) - \sum_{n=1}^N \int_{I_n} ((\mathbf{v} - \mathbf{v}_h) \cdot \nabla \varphi, \psi) dt, \quad (3.17)$$

with $S(\cdot, \cdot)(\cdot)$ being defined in (2.15). Here, $\{\tilde{u}_\tau, \tilde{z}_\tau\} \in X_\tau^{\text{dG}(r)} \times X_\tau^{\text{dG}(r)}$, and $\{\tilde{u}_{\tau h}, \tilde{z}_{\tau h}\} \in X_{\tau h}^{\text{dG}(r),p} \times X_{\tau h}^{\text{dG}(r),p}$ can be chosen arbitrarily and the remainder terms \mathcal{R}_τ and \mathcal{R}_h have the same structure as the remainder term (3.14) in Lemma 3.1.

Remark 3.3. We note that within the spatial error representation formula (3.16b) additional terms due to the coupling occur besides the terms due to stabilization, cf. Eq. (3.17). This is an extension of our previous results obtained in [35], where a convection-dominated transport problem was considered for a given convection tensor not obtained by a Stokes problem that has to be solved additionally, cf. the algorithm described in Sec. 4.

Proof. The proof is related to that one of Thm. 5.2 in [25]. Evaluating the Lagrangian functionals at the respective primal and dual solutions, there holds that

$$J(u) = \mathcal{L}(u, z), \quad J(u_\tau) = \mathcal{L}_\tau(u_\tau, z_\tau), \quad J(u_{\tau h}) = \mathcal{L}_{\tau h}(u_{\tau h}, z_{\tau h}).$$

Since the additional jump terms in \mathcal{L}_τ vanish for a continuous solution $u \in X$, we get the following representation for the temporal and spatial error, respectively,

$$J(u) - J(u_\tau) = \mathcal{L}(u, z) - \mathcal{L}_\tau(u_\tau, z_\tau) = \mathcal{L}_\tau(u, z) - \mathcal{L}_\tau(u_\tau, z_\tau), \quad (3.18a)$$

$$J(u_\tau) - J(u_{\tau h}) = \mathcal{L}_\tau(u_\tau, z_\tau) - \mathcal{L}_{\tau h}(u_{\tau h}, z_{\tau h}). \quad (3.18b)$$

To prove the assertion (3.16a) for the temporal error, we apply Lemma 3.1 with the identifications

$$L = \mathcal{L}_\tau, \quad \tilde{L} = \mathcal{L}_\tau, \quad \mathcal{Y}_1 = X \times X, \quad \mathcal{Y}_2 = X_\tau^{\text{dG}(r)} \times X_\tau^{\text{dG}(r)}$$

to the identity (3.18a). Further, we have to choose $\mathcal{Y} := \mathcal{Y}_1 + \mathcal{Y}_2$ since here $X_\tau^{\text{dG}(r)} \not\subseteq X$. Thus, we have to verify condition (3.12), that now reads as $\mathcal{L}'(u, z)(u_\tau, z_\tau) = 0$, or equivalently,

$$\mathcal{L}'_u(u, z)(u_\tau) = 0 \quad \text{and} \quad \mathcal{L}'_z(u, z)(z_\tau) = 0. \quad (3.19)$$

We only give the proof of the second equation in (3.19). The first one can be proved analogously. To show that $\mathcal{L}'_z(u, z)(z_\tau) = 0$, we rewrite Eq. (3.19) as

$$\sum_{n=1}^N \int_{I_n} \{(g - \rho \partial_t u, z_\tau) - a(u, \mathbf{v})(z_\tau)\} dt = 0.$$

By construction, the continuous solution u satisfies that

$$\int_I \{(\rho \partial_t u, \varphi) + a(u, \mathbf{v})(\varphi)\} dt = \int_I (g, \varphi) dt \quad \forall \varphi \in X. \quad (3.20)$$

Since X is dense in $L^2(I; H_0^1(\Omega))$ with respect to the norm of $L^2(I; H_0^1(\Omega))$ and since no time derivatives of φ arise in (3.20), this equation is also satisfied for all $\varphi \in L^2(I; H_0^1(\Omega))$. The inclusion $z_\tau \in X_\tau^{\text{dG}(r)} \subset L^2(I; H_0^1(\Omega))$ then implies that the second equation in (3.19) is fulfilled.

Now, applying Lemma 3.1 with the above-made identifications yields that

$$\begin{aligned} J(u) - J(u_\tau) &= \mathcal{L}_\tau(u, z) - \mathcal{L}_\tau(u_\tau, z_\tau) \\ &= \frac{1}{2} \mathcal{L}'_\tau(u_\tau, z_\tau)(u - \tilde{u}_\tau, z - \tilde{z}_\tau) + \mathcal{R}_\tau. \end{aligned} \quad (3.21)$$

With the definition of the primal and dual residuals given in (3.15), Eq.(3.21) can be rewritten as

$$J(u) - J(u_\tau) = \frac{1}{2} \rho_t(u_\tau)(z - \tilde{z}_\tau) + \frac{1}{2} \rho_t^*(u_\tau, z_\tau)(u - \tilde{u}_\tau) + \mathcal{R}_\tau,$$

where the remainder term \mathcal{R}_τ is given by

$$\mathcal{R}_\tau = \frac{1}{2} \int_0^1 \mathcal{L}'''_\tau(u_\tau + se, z_\tau + se^*)(e, e, e, e^*, e^*, e^*) s(s-1) ds,$$

with the ‘primal’ and ‘dual’ errors $e := u - u_\tau$ and $e^* := z - z_\tau$, respectively. This proves the assertion (3.16a).

To prove the spatial error representation (3.16b), we apply Lemma 3.1 with the identifications

$$L = \mathcal{L}_\tau, \quad \tilde{L} = \mathcal{L}_{\tau h}, \quad \mathcal{Y}_1 = X_\tau^{\text{dG}(r)} \times X_\tau^{\text{dG}(r)}, \quad \mathcal{Y}_2 = X_{\tau h}^{\text{dG}(r), p} \times X_{\tau h}^{\text{dG}(r), p}$$

to Eq. (3.18b). In this case, we have $\mathcal{Y}_2 \subseteq \mathcal{Y}_1$ since $X_{\tau h}^{\text{dG}(r), p} \subseteq X_\tau^{\text{dG}(r)}$. Hence, we can choose $\mathcal{Y} := \mathcal{Y}_1$ in Lemma 3.1 and condition (3.12) is directly satisfied. Now, applying Lemma 3.1 with these identifications implies that

$$\begin{aligned} J(u_\tau) - J(u_{\tau h}) &= \mathcal{L}_\tau(u_\tau, z_\tau) - \mathcal{L}_{\tau h}(u_{\tau h}, z_{\tau h}) \\ &= \frac{1}{2} \mathcal{L}'_\tau(u_{\tau h}, z_{\tau h})(u_\tau - \tilde{u}_{\tau h}, z_\tau - \tilde{z}_{\tau h}) \\ &\quad + \frac{1}{2} (\mathcal{L}_\tau - \mathcal{L}_{\tau h})'(u_{\tau h}, z_{\tau h})(\tilde{u}_{\tau h} - u_{\tau h}, \tilde{z}_{\tau h} - z_{\tau h}) \\ &\quad + (\mathcal{L}_\tau - \mathcal{L}_{\tau h})(u_{\tau h}, z_{\tau h}) + \mathcal{R}_h. \end{aligned} \quad (3.22)$$

Again, using the definition in (3.15) of the primal and dual residual as well as the definition of $\mathcal{D}_{\tau h}$ given by Eq. (3.17), Eq. (3.22) can be rewritten as

$$\begin{aligned} J(u_\tau) - J(u_{\tau h}) &= \frac{1}{2} \rho_t(u_{\tau h})(z_\tau - \tilde{z}_{\tau h}) + \frac{1}{2} \rho_t^*(u_{\tau h}, z_{\tau h})(u_\tau - \tilde{u}_{\tau h}) \\ &\quad + \frac{1}{2} \mathcal{D}'_{\tau h}(u_{\tau h}, z_{\tau h})(\tilde{u}_{\tau h} - u_{\tau h}, \tilde{z}_{\tau h} - z_{\tau h}) \\ &\quad + \mathcal{D}_{\tau h}(u_{\tau h}, z_{\tau h}) + \mathcal{R}_h, \end{aligned}$$

where the remainder term \mathcal{R}_h is given by

$$\mathcal{R}_h = \frac{1}{2} \int_0^1 \mathcal{L}'''_\tau(u_{\tau h} + se, z_{\tau h} + se^*)(e, e, e, e^*, e^*, e^*) s(s-1) ds,$$

with the ‘primal’ and ‘dual’ errors $e := u_\tau - u_{\tau h}$ and $e^* := z_\tau - z_{\tau h}$. This proves the assertion (3.16b). \square

4. Practical aspects

Here we present the underlying adaptive algorithm, illustrate some practical aspects for the realization of the adaptivity process as well as for the software implementation and give the definition of the (localized) error indicators.

Our space-time adaptivity and mesh refinement strategy uses the following algorithm.

Algorithm: goal-oriented space-time adaptivity

Initialization: Generate the initial space-time slabs $Q_n^1 = \Omega_h^{n,1} \times I_\tau^{n,1}$, $n = 1, \dots, N^1$, with $\bar{I} = \cup_n \bar{I}_\tau^{n,1}$, for the goal-oriented adaptive transport problem.

DWR-loop $\ell = 1, \dots$:

0. Find the solutions $\{\mathbf{v}_h, p_h\} \in Y_h^P$ of the Stokes flow problem (2.2), if the corresponding mesh has changed.
 1. **Find the primal solution** $u_{\tau h} \in X_{\tau h}^{\text{primal}}$ of problem (2.1).
 2. **Break if the goal yields convergence.**
 3. **Find the dual solution** $z_{\tau h} \in X_{\tau h}^{\text{dual}}$ of problem (2.1).
 4. **Evaluate the a posteriori space-time error indicators** η_h and η_τ given by Eq. (4.2) and (4.1), respectively.
 5. **Mark the slabs** $Q_{\tilde{n}}^\ell$, $\tilde{n} \in \{1, \dots, N^\ell\}$, **for temporal refinement** if the corresponding $\eta_\tau^{\tilde{n}}$ is in the set of θ_τ^{top} percent of the worst indicators.
 6. **Mark the cells** $\tilde{K} \in \Omega_h^{n,\ell}$ **for spatial refinement** if the corresponding $\eta_h^n|_{\tilde{K}}$ is in the set of θ_h^{top} percent of the worst indicators, **or**, respectively, **mark for spatial coarsening** if $\eta_h^n|_{\tilde{K}}$ is in the set of θ_h^{bottom} percent of the best indicators.
 7. **Execute spatial adaptations** on all slabs under the use of mesh smoothing operators.
 8. **Execute temporal refinements of slabs.**
 9. Increase ℓ to $\ell + 1$ and return to Step 0.
-

Regarding this algorithm, we note the following issues.

Remark 4.1.

- The primal and dual spaces in the Steps 1 and 3 of the algorithm, $X_{\tau h}^{\text{primal}} = X_{\tau h}^{\text{dG}(r), \text{cG}(p)}$ and $X_{\tau h}^{\text{dual}} = X_{\tau h}^{\text{dG}(s), \text{cG}(q)}$, must be chosen properly, i.e. $p < q$ and $r < s$.
- Within the Steps 1, 3 and 4 of the algorithm, the computed convection field \mathbf{v}_h of the Stokes problem is interpolated to the adaptively refined spatial triangulation of the space-time slabs.
- Technical details of the implementation are given in [30].

A new software, the `dwr-stokes-condiffrea` module of the DTM++ project, was developed for the implementation of the adaptive algorithm. The new module is an extension of the published open-source module `dwr-diffusion` of the DTM++ project; cf. [30]. The extensions are the implementation of the space-time tensor-product finite element spaces for the primal and dual problem on each slab and the coupling of the transport solver to a separated flow module integrated in the software platform. In detail, a tensor product of the d -dimensional spatial finite element space with an one-dimensional temporal finite element space is implemented. The temporal finite element space is based on a discontinuous Galerkin method of arbitrary order r on a one-dimensional triangulation. The temporal triangulation on a space-time slab is shared by the primal and dual problem. The temporal polynomial degree of the primal and dual problem can be chosen arbitrarily. These features enable the full space-time adaptivity our and the flexible choice of polynomial degrees in space and time. Further, the software platform provides an encapsulated flow module, an implementation of a quasi-stationary Stokes problem, that is coupled with a convection-diffusion transport solver. The coupling of the transport and flow solvers is done via the convection tensor field. The latter needs to be interpolated (or projected) from the Stokes solver to the adaptively refined spatial meshes and for the respective degrees of freedom in time on a slab of the transport problem. For the future, this concept enables the realization of multirate, fully space-time adaptive extensions of the current schemes and the incorporation of more sophisticated flow problems. Our simulation tools of the DTM++ project are frontend solvers for the `deal.II` library; cf. [37].

Finally, we give some remarks regarding the localization of the error representations that are derived in Thm. 3.1. Their practical realization and the definition of error indicators η_τ and η_h is obtained by neglecting the remainder terms \mathcal{R}_τ and \mathcal{R}_h of the result given in Thm. 3.1 and splitting the resulting quantities into elementwise contributions.

$$\begin{aligned}
J(u) - J(u_\tau) &\doteq \frac{1}{2} \rho_t^n(u_\tau)(z - \tilde{z}_\tau) + \frac{1}{2} \rho_t^{*,n}(u_\tau, z_\tau)(u - \tilde{u}_\tau) \\
&=: \eta_\tau = \sum_{n=1}^N \eta_\tau^n,
\end{aligned} \tag{4.1}$$

$$\begin{aligned}
J(u_\tau) - J(u_{\tau h}) &\doteq \frac{1}{2} \rho_t^n(u_{\tau h})(z_\tau - \tilde{z}_{\tau h}) + \frac{1}{2} \rho_t^{*,n}(u_{\tau h}, z_{\tau h})(u_\tau - \tilde{u}_{\tau h}) \\
&\quad + \frac{1}{2} \mathcal{D}_{\tau h}'^n(u_{\tau h}, z_{\tau h})(\tilde{u}_{\tau h} - u_{\tau h}, \tilde{z}_{\tau h} - z_{\tau h}) + \mathcal{D}_{\tau h}^n(u_{\tau h}, z_{\tau h}) \\
&=: \eta_h = \sum_{n=0}^N \eta_h^n = \sum_{n=0}^N \sum_{K \in \mathcal{T}_h^n} \eta_{h,K}^n.
\end{aligned} \tag{4.2}$$

To compute the error indicators η_τ and η_h we replace all unknown solutions by the approximated fully discrete solutions $u_{\tau h} \in X_{\tau h}^{\text{dG}(r), \text{cG}(p)}$ and $z_{\tau h} \in X_{\tau h}^{\text{dG}(s), \text{cG}(q)}$, with $r < s$ and $p < q$, whereby the arising weights are approximated in the following way.

- We put $u - \tilde{u}_\tau \approx E_\tau^{r+1}(u_{\tau h}) - u_{\tau h}$ with $E_\tau^{r+1}(\cdot)$ denoting the extrapolation in time operator that acts on a time cell of length τ and lifts the solution to a piecewise polynomial of degree $(r+1)$ in time.

We note that the additional solution for the (local) extrapolation in time on a specific time cell is here interpolated from the previous time cell or the initial condition u_0 in the left end of the time cell. For this, the previous time cell is located on the same slab Q_n^ℓ or the previous one Q_{n-1}^ℓ , where the latter case requires an additional interpolation between two spatial triangulations.

In future works, this concept can be extended to a patchwise higher-order extrapolation in time by using the solutions of two neighboring time cells with an order in time of $(2r+1)$ on the 2τ patch time cell.

- We put $u_\tau - \tilde{u}_{\tau h} \approx E_{2h}^{2p}(u_{\tau h}) - u_{\tau h}$, with $E_{2h}^{2p}(\cdot)$ denoting the extrapolation in space operator that acts on a patched cell of size $2h$ and lifts the solution to a piecewise polynomial of degree $2p$ on the reference cell corresponding to the patched cell of width $2h$.

We note that the extrapolation operator in space is implemented in the `deal.II` library for quadrilateral and hexahedral finite elements and continuous discrete functions of piecewise polynomials with degree p in each variable. The application of this operator requires the spatial triangulation on each slab being at least once globally refined to construct the patched cells of size $2h$. Thereby, an extrapolation degree of at most $2p$ (and not $2p+1$) is due to the shared degrees of freedom on the edges or faces of the continuous FE solution.

- We put $z - \tilde{z}_\tau \approx z_{\tau h} - R_\tau^r(z_{\tau h})$ with $R_\tau^r(\cdot)$ denoting the restriction in time operator on a time cell that restricts the solution to a polynomial of degree $r < s$.

We note that the restriction operator in time is implemented in our software since `deal.II` is currently not able to operate on $(d+1)$ -dimensional tensor-product solutions. This is done by a Lagrangian interpolation in time to the primal space of the dual solution and an additional interpolation back to the dual space.

- We put $z_\tau - \tilde{z}_{\tau h} \approx z_{\tau h} - R_h^p(z_{\tau h})$ with $R_h^p(\cdot)$ denoting the restriction in space operator that acts on a spatial cell and restricts the solution to a polynomial of degree $p < q$ on the corresponding reference cell.

We note that the restriction operator in space is implemented in the `deal.II` library for dimension $d = 2, 3$ as back-interpolation operator between two finite element spaces that are here the dual finite element space and the intermediate primal finite element space.

We recall that within the DWR framework the respective weights have to be approximated using a suitable technique. The most common way for this approximation is the application of a patch-wise higher-order extrapolation; cf. [25, 38, 31]. In this work, the respective operators are chosen in the described manner due to the specific character of linear convection-dominated problems. Our motivation for this results from a comparative study between higher-order extrapolation and higher-order finite element approximations that has been done for a steady-state variant of a convection-dominated problem in [39].

Since we do not consider an analytical solution for the Stokes flow problem (2.2) in some of our numerical examples in Sec. 5, we neglect the coupling terms appearing in (4.2). Instead, we approximate $\{\mathbf{v}_h, p_h\}$ on a sufficiently refined mesh with the Stokes stable finite element pairs $Q_2 - Q_1$ or even $Q_4 - Q_2$ to avoid spatial approximation errors in the transport problem.

For measuring the accuracy of the error estimator, we will study in our numerical convergence experiments (cf. Sec. 5.1) the effectivity index

$$\mathcal{I}_{\text{eff}} = \left| \frac{\eta_\tau + \eta_h}{J(u) - J(u_{\tau h})} \right| \quad (4.3)$$

as the ratio of the estimated error over the exact error. Desirably, the index \mathcal{I}_{eff} should be close to one.

5. Numerical examples

In the following section we study the convergence, computational efficiency and stability of the introduced goal-oriented adaptivity approach for the coupled transport and flow problem. The first example in Sec. 5.1 is an academic problem with a given analytical solution to study the space-time higher-order convergence behavior with a constant convection field for a non-stabilized convection-diffusion transport and a stabilized convection-dominated transport. The lowest-order results can be compared with our preceding published works [35, 30]. The second example in Sec. 5.2 is motivated by problem of physical relevance in which we simulate a convection-dominated transport with goal-oriented adaptivity of a species through a channel with a constraint.

5.1. Example 1 (Stabilized higher-order space-time convergence studies)

This first example is an academic test problem with the given solution

$$\begin{aligned} u(\mathbf{x}, t) &:= u_1 \cdot u_2, \quad \mathbf{x} = (x_1, x_2)^\top \in \mathbb{R}^2 \text{ and } t \in \mathbb{R}, \\ u_1(\mathbf{x}, t) &:= (1 + a \cdot ((x_1 - m_1(t))^2 + (x_2 - m_2(t))^2))^{-1}, \\ u_2(t) &:= \nu_1(t) \cdot s \cdot \arctan(\nu_2(t)), \end{aligned} \quad (5.1)$$

with $m_1(t) := \frac{1}{2} + \frac{1}{4} \cos(2\pi t)$ and $m_2(t) := \frac{1}{2} + \frac{1}{4} \sin(2\pi t)$, and, $\nu_1(\hat{t}) := -1$, $\nu_2(\hat{t}) := 5\pi \cdot (4\hat{t} - 1)$, for $\hat{t} \in [0, 0.5]$ and $\nu_1(\hat{t}) := 1$, $\nu_2(\hat{t}) := 5\pi \cdot (4(\hat{t} - 0.5) - 1)$, for $\hat{t} \in [0.5, 1]$, $\hat{t} = t - k$, $k \in \mathbb{N}_0$, and, scalars $a = 50$ and $s = -\frac{1}{3}$. The (analytic) solution (5.1) mimics a counterclockwise rotating cone which additionally changes its height and orientation over the period $T = 1$. Precisely, the orientation of the cone switches from negative to positive while passing $t = 0.25$ and from positive to negative while passing $t = 0.75$. Exemplary solution profiles at $t = 0$, $t = 0.33$, $t = 0.50$ and $t = 0.85$ are illustrated in Fig. 1.

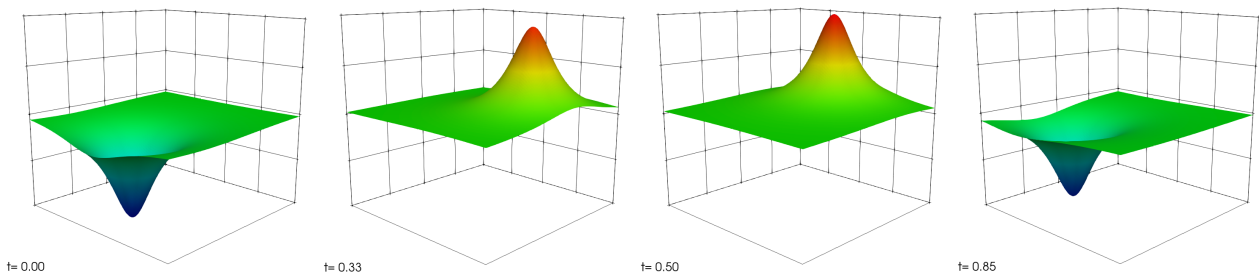


Figure 1: Solution profiles $u_{\tau h}$ at $t = 0$, $t = 0.33$, $t = 0.50$ and $t = 0.85$ for Sec. 5.1.

The right-hand side forcing term g , the inhomogeneous Dirichlet boundary condition and the inhomogeneous initial condition are calculated from the given analytic solution (5.1) and Eqs. (2.1) (a)-(c). Our target quantity is chosen to control the global $L^2(L^2)$ -error of e , $e = u - u_{\tau h}$, in space and time, given by

$$J(\varphi) = \frac{1}{\|e\|_{(0,T) \times \Omega}} \int_I (\varphi, e) dt, \quad \text{with } \|\cdot\|_{(0,T) \times \Omega} = \left(\int_I (\cdot, \cdot) dt \right)^{\frac{1}{2}}. \quad (5.2)$$

The tuning parameters of the goal-oriented adaptive Algorithm given in Sec. 4 are chosen here in a way to balance automatically the potential misfit of the spatial and temporal errors as

$$\theta_h^{\text{top}} = 0.5 \cdot \left| \frac{\eta_h}{\eta_h + \eta_\tau} \right|, \quad \theta_h^{\text{bottom}} = 0 \quad \text{and} \quad \theta_\tau^{\text{top}} = 0.5 \cdot \left| \frac{\eta_\tau}{\eta_h + \eta_\tau} \right|.$$

The convergence behavior, computationally efficiency and stability for higher-order space-time discretizations with and without stabilization is studied in the following of this numerical experiment. Additionally, we compare global against goal-oriented space-time adaptivity. We use here a constant convection field $\mathbf{v} = (2, 3)^\top$ for a non-stabilized convection-diffusion with $\varepsilon = 1$ and $\delta_0 = 0$ transport and a stabilized convection-dominated transport with $\varepsilon = 10^{-6}$ and $\delta_0 = 10^{-1}$ together with the constant reaction coefficient $\alpha = 1$ and the density $\rho = 1$. The local SUPG stabilization coefficient is here $\delta_K = \delta_0 \cdot h_K$ where h_K denotes the cell diameter of the spatial mesh cell K .

ℓ	N	N_K	$N_{\text{DoF}}^{\text{tot}}$	$\ u - u_{\tau h}^{1,1}\ $	EOC	ℓ	N	N_K	$N_{\text{DoF}}^{\text{tot}}$	$\ u - u_{\tau h}^{2,2}\ $	EOC
1	4	4	72	8.7470e-02	—	1	5	4	375	5.3652e-02	—
2	8	16	400	2.7935e-02	1.65	2	10	16	2430	1.3714e-02	1.97
3	16	64	2592	9.0984e-03	1.62	3	20	64	17340	1.5497e-03	3.15
4	32	256	18496	3.0196e-03	1.59	4	40	256	130680	1.9911e-04	2.96
5	64	1024	139392	7.6942e-04	1.97	5	80	1024	1014000	3.5649e-05	2.48
6	128	4096	1081600	1.9290e-04	2.00	6	160	4096	7987680	5.3813e-06	2.73
7	256	16384	8520192	4.9303e-05	1.97	7	320	16384	63407040	6.8615e-07	2.97
8	512	65536	67634176	1.2490e-05	1.98						

Table 1: Global convergence for $u_{\tau h}^{1,1}$ in a cG(1)-dG(1) and $u_{\tau h}^{2,2}$ in a cG(2)-dG(2) primal approximation for a convection-diffusion transport problem with $\varepsilon = 1$ and $\delta_0 = 0$ for Sec. 5.1. ℓ denotes the refinement level, N the total cells in time, N_K the cells in space on a slab, $N_{\text{DoF}}^{\text{tot}}$ the total space-time degrees of freedom, $\|\cdot\|$ the global $L^2(L^2)$ -norm error and EOC the experimental order of convergence.

ℓ	N	N_K	$N_{\text{DoF}}^{\text{tot}}$	$\ u - u_{\tau h}^{1,1}\ $	EOC	ℓ	N	N_K	$N_{\text{DoF}}^{\text{tot}}$	$\ u - u_{\tau h}^{2,2}\ $	EOC
1	4	4	72	5.8984e-02	—	1	4	4	300	4.3801e-02	—
2	8	16	400	4.0001e-02	0.56	2	8	16	1944	1.7138e-02	1.35
3	16	64	2592	1.5534e-02	1.36	3	16	64	13872	7.9707e-03	1.10
4	32	256	18496	6.0496e-03	1.36	4	32	256	104544	3.4451e-03	1.21
5	64	1024	139392	2.2615e-03	1.42	5	64	1024	811200	1.7150e-03	1.01
6	128	4096	1081600	1.0633e-03	1.09	6	128	4096	6390144	8.6229e-04	0.99
7	256	16384	8520192	5.2811e-04	1.01	7	256	16384	50725632	4.3314e-04	0.99
8	512	65536	67634176	2.6493e-04	1.00						

Table 2: Global convergence for $u_{\tau h}^{1,1}$ in a cG(1)-dG(1) and $u_{\tau h}^{2,2}$ in a cG(2)-dG(2) primal approximation for a convection-dominated transport problem with $\varepsilon = 10^{-6}$ and $\delta_0 = 10^{-1}$ for Sec. 5.1. ℓ denotes the refinement level, N the total cells in time, N_K the cells in space on a slab, $N_{\text{DoF}}^{\text{tot}}$ the total space-time degrees of freedom, $\|\cdot\|$ the global $L^2(L^2)$ -norm error and EOC the experimental order of convergence.

Initially, we study the global space-time refinement behavior for the test case with $\varepsilon = 1$ and vanishing stabilization to show the correctness of the higher-order implementation. Therefore, the solution u is approximated with the higher-order in time method cG(1)-dG(1) and with the space-time higher-order method cG(2)-dG(2). Due to the same polynomial orders of the spatial and temporal discretizations, we expect experimental orders of convergence (EOC := $-\log_2(\|e\|_\ell / \|e\|_{\ell-1})$) of $\text{EOC}^{1,1} \approx 2$ for the cG(1)-dG(1) method and $\text{EOC}^{2,2} \approx 3$ for the cG(2)-dG(2) method for a global refinement convergence test. The results are given by Tab. 1 and nicely confirm our expected results for the cG(1)-dG(1) method and roughly confirm the expected results for the cG(2)-dG(2) method. The EOC of the cG(2)-dG(2) is not perfect since the initial space-time errors are not well balanced for this example.

The error reduction of the global space-time refinement results for the convection-dominated case with $\varepsilon = 10^{-6}$ and stabilization with $\delta_0 = 10^{-1}$ are given by Tab. 2. Both methods, that are the cG(1)-dG(1) and the cG(2)-dG(2) approximations of the primal solution $u_{\tau h}$, are limited in their experimental order of convergence of approximately 1. This is not a surprising result since the regularity of the convection-dominated test case is typically of low order. Therefore, we expect further the lower-order or maybe the lowest-order goal-oriented adaptivity methods to perform better than higher-order methods for the convection-dominated test case.

Secondly, we study the goal-oriented space-time adaptivity behavior. Precisely, we compare the solution and dual solution approximation pairings $\{u_{\tau h}, z_{\tau h}\}$: cG(1)-dG(0)/cG(2)-dG(1), cG(1)-dG(1)/cG(2)-dG(2) and cG(2)-dG(2)/cG(3)-dG(3). The lowest-order results can be compared with the results of our preceding published work [35], while remarking that a cG(1)-dG(0)/cG(2)-cG(1) discretization was used there combined with a different choice for the tuning parameters. The results are given by Fig. 2 and by Tab. 3-5. Here, the adaptive method of highest order, i.e. the approximation by cG(2)-dG(2)/cG(3)-dG(3), outperforms all other methods.

Finally, we study the goal-oriented space-time adaptivity behavior for the convection-dominated case with $\varepsilon = 10^{-6}$. Precisely, we compare the solution and dual solution approximation pairings $\{u_{\tau h}, z_{\tau h}\}$: cG(1)-dG(0)/cG(2)-dG(1), cG(1)-dG(1)/cG(2)-dG(2) and cG(2)-dG(2)/cG(3)-dG(3). The lowest-order results can be compared with the results of our preceding published work [35], while remarking that a cG(1)-dG(0)/cG(2)-cG(1) discretization was used there combined with a different choice for the tuning parameters. The results are given by Fig. 3 and by Tab. 6-8. Here, the low order method, but not lowest order, i.e. the approximation by cG(1)-dG(1)/cG(2)-dG(2), outperforms all other methods.

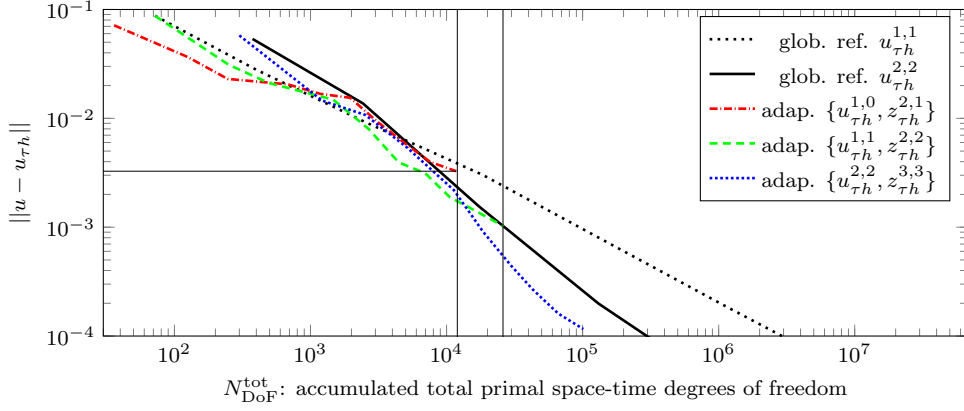


Figure 2: $L^2(L^2)$ -error reduction in the convection-diffusion transport case with $\varepsilon = 1$ without stabilization $\delta_0 = 0$ for Sec. 5.1. The solution approximations are $u_{\tau h}^{1,0}$ in cG(1)-dG(0), $u_{\tau h}^{1,1}$ in cG(1)-dG(1), $u_{\tau h}^{2,2}$ in cG(2)-dG(2) and the dual solution approximations are $z_{\tau h}^{2,1}$ in cG(2)-dG(1), $z_{\tau h}^{2,2}$ in cG(2)-dG(2), $z_{\tau h}^{3,3}$ in cG(3)-dG(3).

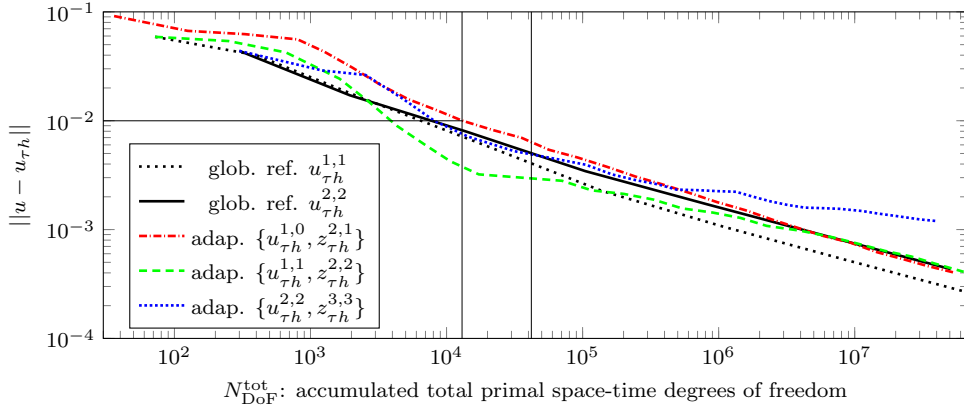


Figure 3: $L^2(L^2)$ -error reduction in the stabilized convection-dominated transport case with $\varepsilon = 10^{-6}$ and $\delta_0 = 10^{-1}$ for Sec. 5.1. The solution approximations are $u_{\tau h}^{1,0}$ in cG(1)-dG(0), $u_{\tau h}^{1,1}$ in cG(1)-dG(1), $u_{\tau h}^{2,2}$ in cG(2)-dG(2) and the dual solution approximations are $z_{\tau h}^{2,1}$ in cG(2)-dG(1), $z_{\tau h}^{2,2}$ in cG(2)-dG(2), $z_{\tau h}^{3,3}$ in cG(3)-dG(3).

ℓ	N	N_K^{\max}	$N_{\text{DoF}}^{\text{tot}}$	$\ e^{1,0,2,1}\ $	EOC	η_h	η_τ	$\eta_{\tau h}$	\mathcal{I}_{eff}
1	4	4	36	7.1588e-02	—	5.6668e-02	1.9391e-02	7.6060e-02	1.062
2	5	16	125	3.6641e-02	0.97	7.4575e-03	2.8043e-02	3.5501e-02	0.969
3	6	28	246	2.3021e-02	0.67	5.4712e-03	3.2327e-02	3.7798e-02	1.642
4	8	76	682	2.0517e-02	0.17	2.1734e-03	2.0763e-02	2.2936e-02	1.118
5	11	88	1181	1.6786e-02	0.29	2.3597e-03	2.1533e-02	2.3892e-02	1.423
6	15	124	1959	1.5438e-02	0.12	1.4977e-03	1.4946e-02	1.6443e-02	1.065
7	21	136	3085	9.3565e-03	0.72	2.3671e-03	1.5271e-02	1.7638e-02	1.885
8	30	160	4878	5.9652e-03	0.65	2.5744e-03	1.2993e-02	1.5567e-02	2.610
9	42	172	7610	3.9673e-03	0.59	2.1052e-03	7.8182e-03	9.9234e-03	2.501
10	58	208	11786	3.2686e-03	0.28	2.4333e-03	6.3257e-03	8.7590e-03	2.680
				avg. EOC =	0.50				

Table 3: $L^2(L^2)$ -error reduction in the convection-diffusion transport case with $\varepsilon = 1$ without stabilization $\delta_0 = 0$ for Sec. 5.1. $e^{1,0,2,1}$ corresponds to the adaptive solution approximation $u_{\tau h}^{1,0}$ in cG(1)-dG(0) and dual solution approximation $z_{\tau h}^{2,1}$ in cG(2)-dG(1).

ℓ	N	N_K^{\max}	$N_{\text{DoF}}^{\text{tot}}$	$\ e^{1,1,2,2}\ $	EOC	η_h	η_τ	$\eta_{\tau h}$	\mathcal{I}_{eff}
1	4	4	72	8.7470e-02	—	4.7959e-02	-4.5912e-03	4.3367e-02	0.496
2	5	16	250	3.1113e-02	1.49	4.1953e-03	7.3543e-03	1.1550e-02	0.371
3	6	28	492	2.1156e-02	0.56	3.0706e-03	9.2354e-03	1.2306e-02	0.582
4	8	76	1468	1.4856e-02	0.51	2.1015e-03	6.4001e-03	8.5016e-03	0.572
5	11	124	2666	8.0165e-03	0.89	2.6080e-03	6.5137e-03	9.1217e-03	1.138
6	14	160	4456	3.9318e-03	1.03	3.1048e-03	7.1463e-03	1.0251e-02	2.607
7	18	196	6960	3.1346e-03	0.33	2.2002e-03	4.3348e-03	6.5350e-03	2.085
8	23	232	10610	1.8780e-03	0.74	5.4403e-04	1.7686e-03	2.3126e-03	1.231
9	31	280	16522	1.4014e-03	0.42	3.5661e-04	9.3709e-04	1.2937e-03	0.923
10	42	340	26252	1.0214e-03	0.46	5.1205e-05	2.8010e-04	3.3130e-04	0.324
				avg. EOC =	0.71				

Table 4: $L^2(L^2)$ -error reduction in the convection-diffusion transport case with $\varepsilon = 1$ without stabilization $\delta_0 = 0$ for Sec. 5.1. $e^{1,1,2,2}$ corresponds to the adaptive solution approximation $u_{\tau h}^{1,1}$ in cG(1)-dG(1) and dual solution approximation $z_{\tau h}^{2,2}$ in cG(2)-dG(2).

ℓ	N	N_K^{\max}	$N_{\text{DoF}}^{\text{tot}}$	$\ e^{2,2,3,3}\ $	EOC	η_h	η_τ	$\eta_{\tau h}$	\mathcal{I}_{eff}
1	4	4	300	5.7763e-02	—	4.1837e-03	3.6501e-03	7.8339e-03	0.136
2	5	16	1215	1.4581e-02	1.99	3.5634e-03	4.5982e-03	8.1616e-03	0.560
3	6	28	2538	1.0721e-02	0.44	5.9011e-04	4.9905e-03	5.5806e-03	0.521
4	8	76	5112	5.4041e-03	0.99	3.0895e-04	3.3977e-03	3.7067e-03	0.686
5	11	88	11325	2.1878e-03	1.30	6.4201e-04	2.7536e-03	3.3956e-03	1.552
6	15	100	18489	9.1402e-04	1.26	4.6743e-04	1.8813e-03	2.3487e-03	2.570
7	21	124	29895	4.4147e-04	1.05	3.3121e-04	1.9212e-04	5.2333e-04	1.185
8	24	184	43026	2.6759e-04	0.72	1.5650e-04	1.7675e-04	3.3325e-04	1.245
9	30	208	66270	1.6078e-04	0.73	7.4964e-05	1.5182e-04	2.2678e-04	1.410
10	40	256	101178	1.1594e-04	0.47	6.7057e-05	1.9555e-05	8.6611e-05	0.747
				avg. EOC =	0.99				

Table 5: $L^2(L^2)$ -error reduction in the convection-diffusion transport case with $\varepsilon = 1$ without stabilization $\delta_0 = 0$ for Sec. 5.1. $e^{2,2,3,3}$ corresponds to the adaptive solution approximation $u_{\tau h}^{2,2}$ in cG(2)-dG(2) and dual solution approximation $z_{\tau h}^{3,3}$ in cG(3)-dG(3).

ℓ	N	N_K^{\max}	$N_{\text{DoF}}^{\text{tot}}$	$\ e^{1,0,2,1}\ $	EOC	η_h	η_τ	$\eta_{\tau h}$	\mathcal{I}_{eff}
1	4	4	36	9.1527e-02	—	3.6697e-02	1.5147e-02	5.1844e-02	0.566
2	5	16	125	6.6916e-02	0.45	6.4515e-03	-6.0024e-04	5.8513e-03	0.087
3	6	52	330	6.2426e-02	0.10	2.6882e-03	5.9916e-03	8.6798e-03	0.139
4	8	88	804	5.5849e-02	0.16	2.1670e-03	6.6884e-03	8.8554e-03	0.159
5	11	100	1265	4.3011e-02	0.38	3.2302e-03	1.1793e-02	1.5023e-02	0.349
6	15	124	2037	3.0684e-02	0.49	2.3297e-03	1.3276e-02	1.5605e-02	0.509
7	21	160	3283	2.1294e-02	0.53	1.8278e-03	1.1939e-02	1.3767e-02	0.647
8	30	184	5262	1.5710e-02	0.44	2.7619e-03	1.0873e-02	1.3635e-02	0.868
9	41	220	8357	1.2567e-02	0.32	3.3126e-03	7.9147e-03	1.1227e-02	0.893
10	55	280	13121	9.9855e-03	0.33	5.5998e-03	6.5796e-03	1.2179e-02	1.220
				avg. EOC =	0.36				

Table 6: $L^2(L^2)$ -error reduction in the stabilized convection-dominated transport case with $\varepsilon = 10^{-6}$ and $\delta_0 = 10^{-1}$ for Sec. 5.1. $e^{1,0,2,1}$ corresponds to the adaptive solution approximation $u_{\tau h}^{1,0}$ in cG(1)-dG(0) and dual solution approximation $z_{\tau h}^{2,1}$ in cG(2)-dG(1).

ℓ	N	N_K^{\max}	$N_{\text{DoF}}^{\text{tot}}$	$\ e^{1,1,2,2}\ $	EOC	η_h	η_τ	$\eta_{\tau h}$	\mathcal{I}_{eff}
1	4	4	72	5.8984e-02	—	2.6394e-02	1.3546e-03	2.7749e-02	0.470
2	5	16	250	5.3935e-02	0.13	-1.4730e-02	3.8407e-03	-1.0889e-02	0.202
3	6	52	660	4.2387e-02	0.35	-5.4370e-04	4.7724e-03	4.2287e-03	0.100
4	9	76	1634	2.4328e-02	0.80	1.2300e-03	4.5411e-03	5.7711e-03	0.237
5	12	124	2668	1.5031e-02	0.69	7.6984e-03	4.4589e-03	1.2157e-02	0.809
6	14	172	4316	8.9709e-03	0.74	2.7195e-03	5.1674e-03	7.8869e-03	0.879
7	18	208	7032	5.9470e-03	0.59	3.2797e-03	3.1406e-03	6.4202e-03	1.080
8	22	268	10668	4.2404e-03	0.49	-1.1081e-04	1.7962e-03	1.6854e-03	0.397
9	33	292	17270	3.2138e-03	0.40	-1.8817e-03	7.9462e-04	-1.0871e-03	0.338
10	45	568	41550	2.9555e-03	0.12	-8.4016e-03	3.2177e-04	-8.0798e-03	2.734
				avg. EOC =	0.48				

Table 7: $L^2(L^2)$ -error reduction in the stabilized convection-dominated transport case with $\varepsilon = 10^{-6}$ and $\delta_0 = 10^{-1}$ for Sec. 5.1. $e^{1,1,2,2}$ corresponds to the adaptive solution approximation $u_{\tau h}^{1,1}$ in cG(1)-dG(1) and dual solution approximation $z_{\tau h}^{2,2}$ in cG(2)-dG(2).

ℓ	N	N_K^{\max}	$N_{\text{DoF}}^{\text{tot}}$	$\ e^{2,2,3,3}\ $	EOC	η_h	η_τ	$\eta_{\tau h}$	\mathcal{I}_{eff}
1	4	4	300	4.3801e-02	—	-2.6854e-03	1.0697e-03	-1.6156e-03	0.037
2	5	16	1215	2.8964e-02	0.60	2.2071e-03	2.3582e-03	4.5653e-03	0.158
3	6	28	2538	2.6314e-02	0.14	1.0415e-03	2.0664e-03	3.1078e-03	0.118
4	7	76	4719	1.6058e-02	0.71	6.6330e-04	2.2853e-03	2.9486e-03	0.184
5	9	88	8175	9.9382e-03	0.69	4.8613e-04	1.9507e-03	2.4369e-03	0.245
6	12	124	14442	7.1355e-03	0.48	-5.9480e-04	1.0807e-03	4.8594e-04	0.068
7	18	244	31548	5.2461e-03	0.44	-1.7721e-03	6.0417e-04	-1.1680e-03	0.223
8	22	376	66042	4.4188e-03	0.25	-1.1307e-03	1.0326e-04	-1.0275e-03	0.233
9	23	556	105825	3.9399e-03	0.17	-1.3787e-03	-8.2448e-05	-1.4611e-03	0.371
10	24	868	164886	3.2102e-03	0.30	-1.0300e-03	-1.4457e-04	-1.1746e-03	0.366
				avg. EOC =	0.42				

Table 8: $L^2(L^2)$ -error reduction in the stabilized convection-dominated transport case with $\varepsilon = 10^{-6}$ and $\delta_0 = 10^{-1}$ for Sec. 5.1. $e^{2,2,3,3}$ corresponds to the adaptive solution approximation $u_{\tau h}^{2,2}$ in cG(2)-dG(2) and dual solution approximation $z_{\tau h}^{3,3}$ in cG(3)-dG(3).

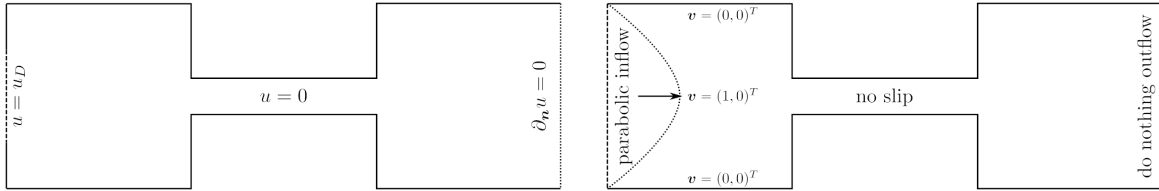


Figure 4: Boundary colorization for the convection-diffusion problem (left) and the coupled Stokes problem (right) for Sec. 5.2.

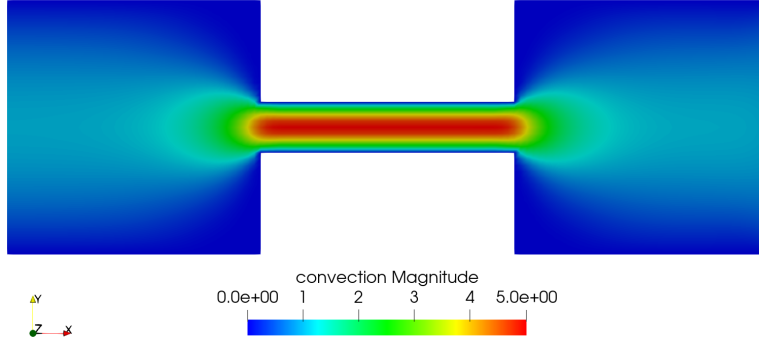


Figure 5: Convection v_h solution of the Stokes problem on a sufficiently globally refined mesh with Q_2 - Q_1 finite elements for Sec. 5.2. On the left boundary a parabolic inflow profile in the positive x -direction with unit magnitude is prescribed for the convection v .

5.2. Example 2 (Transport in a channel)

In this example we simulate a convection-dominated transport with goal-oriented adaptivity of a species through a channel with a constraint. The domain and its boundary colorization are presented by Fig. 4. Precisely, the spatial domain is composed of two unit squares and a constraint in the middle which restricts the channel height by a factor of 5. Precisely, $\Omega = (-1, 0) \times (-0.5, 0.5) \cup (0, 1) \times (-0.1, 0.1) \cup (1, 2) \times (-0.5, 0.5)$ with an initial cell diameter of $h = \sqrt{2 \cdot 0.025^2}$. The time domain is set to $I = (0, 2.5)$ with an initial $\tau = 0.1$ for the initialization of the slabs for the first loop $\ell = 1$. We approximate the primal solution $u_{\tau h}^{1,1}$ with the cG(1)-dG(1) method and the dual solution $z_{\tau h}^{2,2}$ with the cG(2)-dG(2) method. The target quantity is

$$J(\varphi) = \frac{1}{\|u_{\tau h}\|_{(0,T) \times \Omega}} \int_I (\varphi, u_{\tau h}) dt.$$

The transport of the species, which enters the domain on the left with an inhomogeneous and time-dependent Dirichlet boundary condition and leaves the domain on the right through a homogeneous Neumann boundary condition, is driven by the convection with magnitudes between 0 and 5 as displayed in Fig. 5. The diffusion coefficient has the constant and small value of $\varepsilon = 10^{-4}$, the reaction coefficient $\alpha = 0$ is vanishing and the density has the value $\rho = 1$. The local SUPG stabilization coefficient is here set to $\delta_K = \delta_0 \cdot h_K$, $\delta_0 = 0$, i.e. a vanishing stabilization here. The initial value function $u_0 = 0$ as well as the forcing term $g = 0$ are homogeneous. The Dirichlet boundary function value is homogeneous on Γ_D except for the line $(-1, -1) \times (-0.25, 0.25)$ where the value

$$u(y, t) = 16 \cdot (0.25 - y) \cdot (y + 0.25) \cdot \min\{100t, 0.1\}$$

is prescribed on the solution. The viscosity is set to $\tilde{\nu} = 1$. The tuning parameters of the goal-oriented adaptive Algorithm given in Sec. 4 are chosen here in a way to balance automatically the potential misfit of the spatial and temporal errors as $\theta_h^{\text{bottom}} = 0$,

$$\theta_h^{\text{top}} = \frac{1}{2} \cdot \min \left\{ \left| \frac{\eta_h}{\eta_h + \eta_\tau} \right|, 1 \right\} \quad \text{and} \quad \theta_\tau^{\text{top}} = \frac{1}{2} \cdot \min \left\{ \left| \frac{\eta_\tau}{\eta_h + \eta_\tau} \right|, 1 \right\}. \quad (5.3)$$

The solution profiles and corresponding adaptive meshes of the primal solution $u_{\tau h}^{1,1}$ of the loop $\ell = 5$ for $t = 0.82$, $t = 1.32$ and $t = 2.28$ are given by Fig. 6. In Fig. 7 we present a comparative study of the solution profile and corresponding meshes for $t = 1.21$ over the adaptivity loops. For $\ell = 1, 2, 3$ obvious spurious oscillations in the left square are existing, which are captured and resolved by the goal-oriented adaptivity by taking spatial mesh refinements next to the right boundary of the left square. For $\ell > 3$ the spatial refinements capture especially the solution profile fronts with strong gradients with a focus on the high-convective middle of the spatial domain. The refinement in space and time is automatically balanced due to the dynamic choice of θ_h^{top} and θ_τ^{top} given by (5.3) and is illustrated by Tab. 9. Precisely, the space-time mesh updates for the loops 2-8 are dominated by spatial refinements while a significant growth of the time elements can be recognized for the 9th loop.

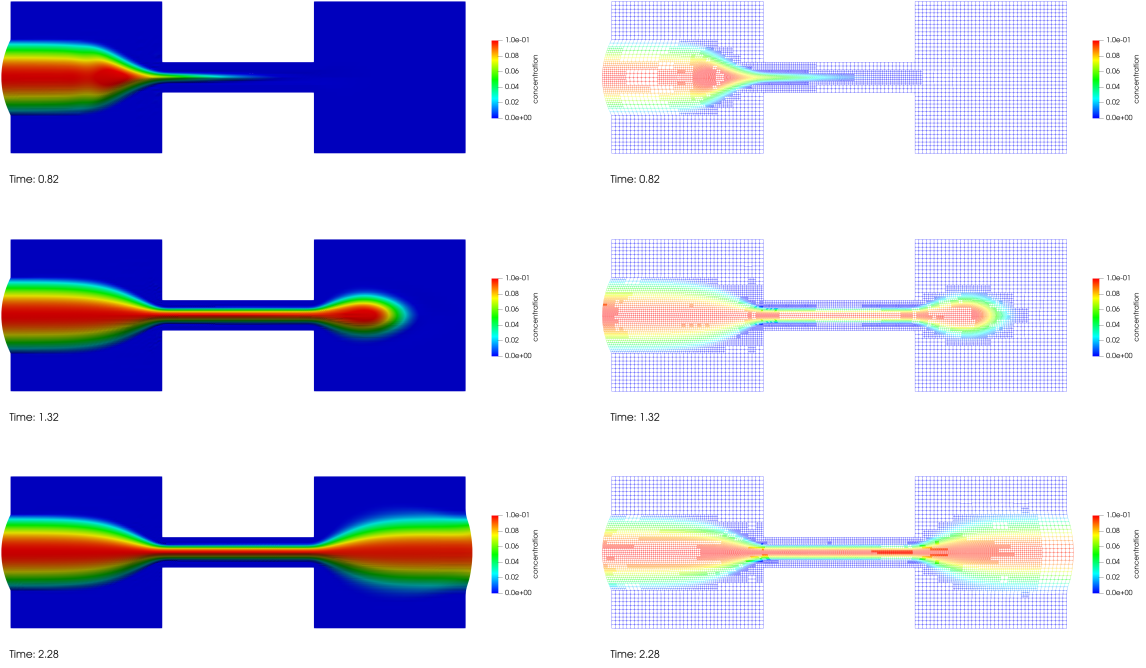


Figure 6: Solution profiles and corresponding meshes of loop $\ell = 5$ for Sec. 5.2.

ℓ	N	N_K^{tot}	N_K^{max}	$\ u_{\tau h}^{1,1}\ $
1	25	88000	3520	0.0845694
2	26	108380	5008	0.0843620
3	27	153324	8464	0.0844429
4	28	203524	10792	0.0845339
5	29	298952	17680	0.0846325
6	30	459696	25996	0.0847412
7	31	649852	38212	0.0848211
8	32	1058456	68344	0.0848755
9	41	1881548	100744	0.0849878

Table 9: Goal-oriented temporal and spatial refinements for Sec. 5.2. ℓ denotes the refinement level loop, N the accumulated total cells in time, N_K^{tot} the accumulated total cells in space, N_K^{max} the maximal number of cells on a slab and $\|u_{\tau h}^{1,1}\|$ the value of the goal-functional.

6. Summary

In this work we presented a space-time adaptive solution algorithm for SUPG stabilized finite element approximations of a convection-dominated transport problem that is coupled with a flow problem. The convection-dominance puts further facets of complexity and sensitivity on the a posteriori error control, but also illustrates the efficiency and potential of automatic mesh adaptation. The underlying approach is based on the Dual Weighted Residual method for goal-oriented error control. A splitting of the discretization errors in space and time is used for the transport problem which is then used for the respective mesh adaptation process in the form of underlying error indicators η_τ and η_h , respectively. A discontinuous Galerkin method $\text{dG}(r)$ with an arbitrary polynomial degree $r \geq 0$ is applied for the discretization in time of the transport problem. The weights of the DWR adaptivity process are approximated by higher-order finite elements instead of using patch-wise higher-order extrapolation. In numerical experiments we could prove that spurious oscillations that typically arise in numerical approximations of convection-dominated problems could be reduced significantly. Effectivity indices close to one were obtained for small diffusion coefficients corresponding to high Péclet numbers. Moreover, the potential of the approach was illustrated for a problem of practical interest. Along with the underlying software platform, even more sophisticated techniques and settings including multirate approximations, varying meshes for flow and transport or coupling with time-dependent flow problems become feasible.

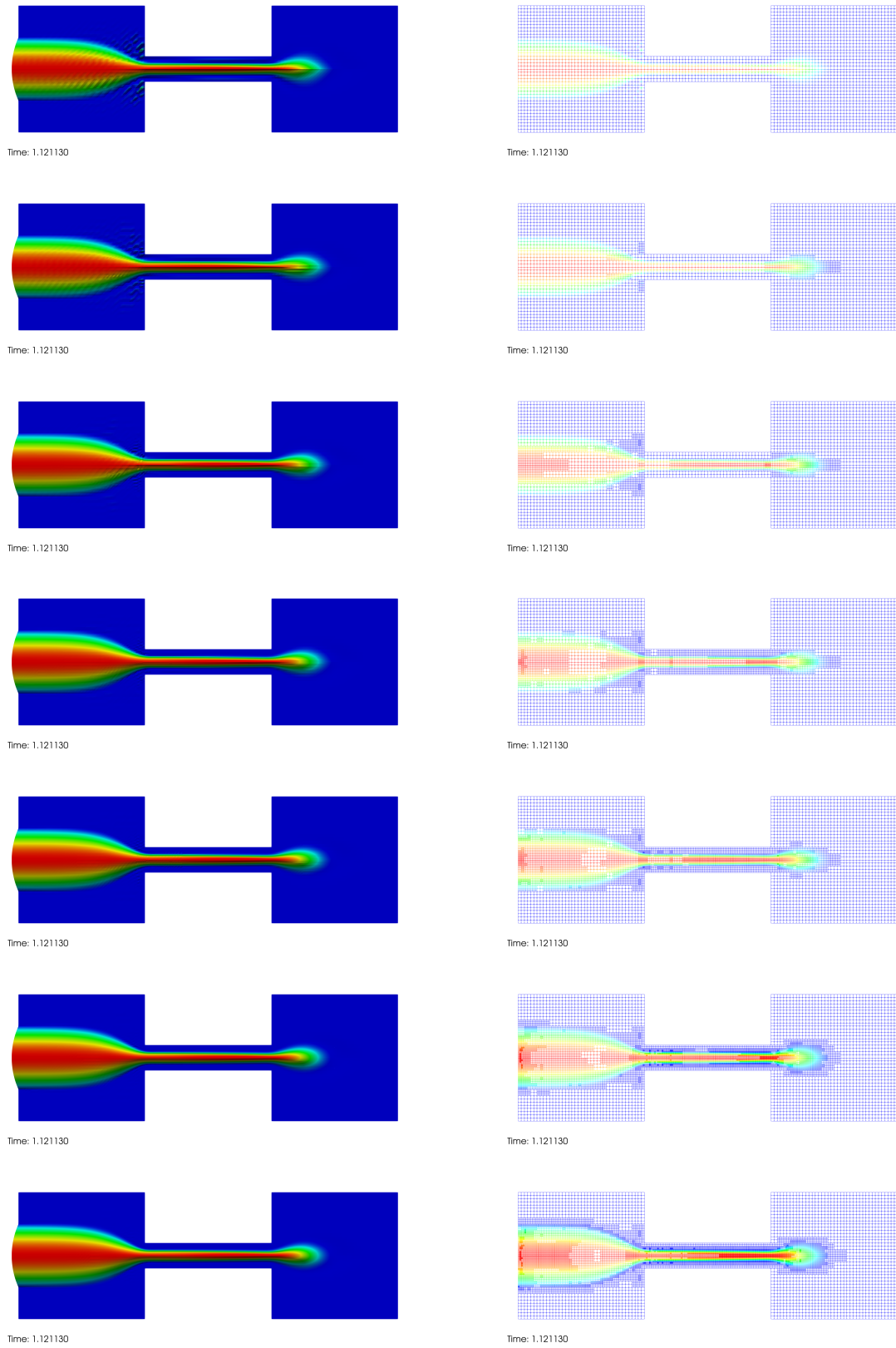


Figure 7: Capturing of spurious oscillations with goal-oriented adaptivity illustrated by comparative solution profiles and corresponding meshes of the loops $\ell = 1 - 7$ for Sec. 5.2.

Acknowledgements

U. Köcher was partially supported by the Oden Institute for Computational Engineering and Sciences, University of Texas at Austin, Texas, USA as long-term guest visitor of M.F. Wheeler for the implementation of the used space-time-slab finite element handler.

References

- [1] Larson, M.G., Malquist, A.: Goal oriented adaptivity for coupled flow and transport with applications in oil reservoir simulations. *Comput. Methods Appl. Mech. Engrg.* **196**, 3546–3561 (2007)
- [2] Biot, M.A.: General theory of three-dimensional consolidation. *J. Appl. Phys.* **12**(2), 155-164, doi:10.1063/1.1712886, (1941)
- [3] Allaire, G.: Homogenization of the Stokes flow in a connected porous medium. *Asymptotic Anal.* **2**, 203-222, (1989)
- [4] Showalter, R.: Diffusion in poro-elastic media. *J. Math. Anal. Appl.* **251**, 310–340 (2000)
- [5] Almani, T., Kumar, K., Dogru, A., Singh, G., Wheeler, M.F.: Convergence analysis of multirate fixed-stress split iterative schemes for coupling flow with geomechanics. *Comput. Meth. Appl. Mech. Engrg.* **311**, 180–207 (2016)
- [6] Ge, Z., Ma, M.: Multiphysics discontinuous Galerkin method for a poroelasticity model. *Appl. Math. Comput.* **301**, 78–94 (2017)
- [7] Wick, T.: Goal functional evaluations for phase-field fracture using PU-based DWR mesh adaptivity. *Comput. Mech.* **57**, 1017–1035 (2016)
- [8] Odsæter, L.H., Kvamsdal, T., Larson, M.G.: A simple embedded discrete fracture-matrix model for a coupled flow and transport problem in porous media. *Comp. Methods Appl. Mech. Engrg.* **343**, 572-601 (2019)
- [9] Ge, Z., Ma, M.: Multirate iterative scheme based on mutiphysics discontinuous Galerkin method for a poroelasticity model. *Appl. Numer. Math.* **128**, 125–138 (2018)
- [10] Gupta, S., Wohlmuth, B., Helmig, R.: Multirate time stepping schemes for hydro-geomechanical model for subsurface methane hydrate reservoirs. *Adv Water Res.* **91**, 78–87 (2016)
- [11] Mikelić, A., Wheeler, M.F.: Convergence of iterative coupling for coupled flow and geomechanics. *Comput. Geosci.* **17**, 479–496 (2013)
- [12] John, V., Knobloch, P., Novo, J.: Finite elements for scalar convection-dominated equations and incompressible flow problems: a never ending story? *Comput. Vis. Sci.*, doi:10.1007/s00791-018-0290-5, 1–17 (2018)
- [13] John, V., Schmeyer, E.: Finite element methods for time-dependent convection-diffusion-reaction equations with small diffusion. *Comput. Methods Appl. Mech. Engrg.* **198**, 173–181 (2009)
- [14] Roos, H.-G., Stynes, M., Tobiska, L.: *Robust Numerical Methods for Singularly Perturbed Differential Equations.* Springer, Berlin (2008)
- [15] Ainsworth, M., Oden, J. T.: *A posteriori error estimation in finite element analysis.* Wiley, New York (2000)
- [16] Verfürth, R.: *A Review of A Posteriori Error Estimation and Adaptive Mesh-Refinement Techniques.* Wiley-Teubner Series Advances in Numerical Mathematics. Wiley-Teubner, New York Stuttgart (1996)
- [17] Becker, R., Rannacher, R.: A feed-back approach to error control in finite element methods: Basic analysis and examples. *East-West J. Numer. Math.* **4**, 237–264 (1996)
- [18] Becker, R., Rannacher, R.: Weighted a posteriori error control in FE methods. In: Bock, H. G. et al. (eds.) ENUMATH 97. Proceedings of the 2nd European Conference on Numerical Mathematics and Advanced Applications, pp. 621–637. World Scientific, Singapore (1998)
- [19] Becker, R., Rannacher, R.: An optimal control approach to a posteriori error estimation in finite element methods. In: Iserles, A. (ed.) *Acta Numer.*, vol. 10, pp. 1–102. Cambridge University Press (2001)

- [20] Rannacher, R., Vihharev, J.: Adaptive finite element analysis of nonlinear problems: balancing of discretization and iteration errors. *J. Numer. Math.* **21**, 23–61 (2013)
- [21] Braack, M., Ern, A.: A posteriori control of modeling errors and discretization errors. *Multiscale Model. Simul.* **1**, 221–238 (2003)
- [22] Endtmayer, B., Wick, T.: A partition-of-unity dual-weighted residual approach for multiple objective goal functional error estimation applied to elliptic problems. *Comput. Methods Appl. Math.* **17**, 575–599 (2017)
- [23] Endtmayer, B., Langer, U., Wick, T.: Two-side a posteriori error estimates for the DWR method, *SIAM J. Sci. Comput.*, in press (2019); arXiv:1811.07586
- [24] Bangerth, W., Rannacher, R.: Adaptive finite element methods for differential equations. Birkhäuser, Basel (2003)
- [25] Besier, M., Rannacher, R.: Goal-oriented space-time adaptivity in the finite element Galerkin method for the computation of nonstationary incompressible flow. *Int. J. Num. Methods Fluids* **70**(9), 1139–1166 (2012)
- [26] Meidner, D., Richter, T.: A posteriori error estimation for the fractional step theta discretization of the incompressible NavierStokes equations. *Comput. Methods Appl. Mech. Eng.* **288**, 45–59, doi:10.1016/j.cma.2014.11.031 (2015)
- [27] Richter, T.: Fluid–Structure Interactions: Models, Analysis and Finite Elements, Lecture Notes in Computational Science and Engineering, vol. 118. Springer, Berlin (2017)
- [28] Failer, L., Wick, T.: Adaptive time-step control for nonlinear fluidstructure interaction. *J. Comput. Phys.* **366**, 448–477, doi:10.1016/j.jcp.2018.04.021 (2018)
- [29] Richter, T.: Goal-oriented error estimation for fluidstructure interaction problems. *Comput. Methods Appl. Mech. Eng.* **223–224**, 28–42, doi:10.1016/j.cma.2012.02.014 (2012)
- [30] Köcher, U., Bruchhäuser, M. P., Bause, M.: Efficient and scalable data structures and algorithms for goal-oriented adaptivity of space-time FEM codes. *SoftwareX* **10**:1-6, 100239, doi:10.1016/j.softx.2019.100239, in press (2019)
- [31] Schmich, M., Vexler, B.: Adaptivity with dynamic meshes for space-time finite element discretizations of parabolic equations. *SIAM J. Sci. Comput.* **30**, 369–393 (2008)
- [32] Carey, G. F., Oden, J. T.: Finite Elements, Computational Aspects, Vol. III (The Texas finite element series). Prentice-Hall, Englewood Cliffs, New Jersey (1984)
- [33] Hughes, T. J. R., Brooks, A. N.: A multidimensional upwind scheme with no crosswind diffusion. In: Hughes, T. J. R. (eds.) *Finite Element Methods for Convection Dominated Flows*, AMD, vol. 34, pp. 19–35. Amer. Soc. Mech. Engrs. (ASME) (1979)
- [34] Brooks, A. N., Hughes, T. J. R.: Streamline upwind/Petrov-Galerkin formulations for convection dominated flows with particular emphasis on the incompressible Navier-Stokes equations. *Comput. Methods Appl. Mech. Engrg.* **32**(1-3), 199–259 (1982)
- [35] Bruchhäuser, M. P., Schwegler, K., Bause, M.: Dual weighted residual based error control for nonstationary convection-dominated equations: potential or ballast? In Barrenechea G. R., Mackenzie, J. (eds.), *Boundary and Interior Layers, Computational and Asymptotic Methods BAIL 2018*, Lecture Notes in Computational Science and Engineering **135**, Springer, doi:10.1007/978-3-030-41800-7_1 (2020)
- [36] John, V., Novo, J.: Error analysis of the SUPG finite element discretization of evolutionary convection-diffusion-reaction equations. *SIAM J. Numer. Anal.* **49**(3), 1149–1176 (2011)
- [37] Arndt, D., Bangerth, W., Clevenger, T., Davydov, D., Fehling, M., Garcia-Sanchez, D., Harper, G., Heister, T., Heltai, L., Kronbichler, M., Maguire Kynch, R., Maier, M., Pelteret, J.P., Turcksin, B., Wells, D.: *The deal.II Library*, Version 9.1, *J. Numer. Math.* (2019). doi:10.1515/jnma-2019-0064, pp. 1–14.
- [38] Bangerth, W., Geiger, M., Rannacher, R.: Adaptive Galerkin finite element methods for the wave equation. *Comput. Meth. Appl. Math.* **10**, 3–48 (2010)
- [39] Bruchhäuser, M. P., Schwegler, K., Bause, M.: Numerical study of goal-oriented error control for stabilized finite element methods. In Apel, T. et al. (eds.) *Advanced Finite Element Methods with Applications. FEM 2017*, Lecture Notes in Computational Science and Engineering **128**, Springer, Cham, 2019, 85–106 doi:10.1007/978-3-030-14244-5_5, (2019)